NEW HIGH FLEXIBLE STAINLESS STEEL PROCESS LINE WITH ADVANCED PROCESS CONTROL AT BAOSTEEL SHANGHAI NO.1 / PR CHINA

S. Guomin[1], J. Kempken[2], J. Reichel[2]

[1]BGYG PR, China, [2]SMS Demag, AG, Germany

Introduction

Driven by stainless steel production technologies and market demand, the compound annual growth rate of stainless crude steel production has during the last 50 years risen on average by 6% every 10 years. China has become the main force in consuming the world's stainless steel resource surplus and is gradually becoming the world's main market for stainless steel in which companies are competing. On the basis of economic analyses of the stainless steel market it can be stated that China´s stainless steel production capacity surplus will exceed 20% by 2010. One of the significant events not only in view of the development of the Baosteel Group itself but also on a domestic and international scale and China´s position in the production of stainless steel was the award in August 2001 to the Consortium of SMS Demag AG, Siemens and TK Stainless of a contract for setting up a complete state-of-the-art production line for stainless steel consisting of DDD, EAF, AOD, VOD and CCM equipment. The complete package including the engineering, supply and supervision for erection and start-up was the responsibility of the consortium under the general management of SMS Demag AG.

In May 2004, Baosteel Group commissioned a hot strip stainless steel meltshop with a designed production capacity of:

- liquid stainless steel 0.75m tpy
- stainless steel slabs 0.72m tpy
- stainless steel strip coils 0.587m tpy

With the second phase of this project erected in December 2004, Shanghai No. 1 has extended its production capacity and is now one of the world's largest producers of stainless steel flat products.

-

On June 18, 2005, hot test runs with of the meltshop expansion project were successfully completed with:

liquid stainless steel 1.5m tpy
stainless steel slabs 1.44m tpy
stainless steel strip coils 1.287m tpy

Since this time Shanghai No. 1, Figure1, a member of the Baosteel Group, is now one of the biggest flat stainless steel producers in the PR China and in the world.
The modern plant layout, the design of ancillary equipment and ladle logistic systems shorten liquid material handling and save valuable energy.

The EAF operates only as melting unit. The next process step is performed in the AOD converter with top lance and, depending on the required steel grade, in the VOD/LTS facility to comply with the high quality requirements for stainless steel products.
The core equipment consists of:

: Hot-metal Treatment Station (DDD) Sumitomo Technology
: 1 x 100t / 120t AC EAF with scrap handling equipment
: 1 x 120t /135t AOD-L converter with ancillary equipment
: 1 x 120t SS-VOD / LTS unit
: 1 x CCM
: Ladle skimming and treatment facilities
: Ladle preparation and repair facilities
: Alloy and dust handling facilities

Figure1 Steel plant Shanghai No1. Baosteel Group

Production program

The production of ferritic and austenitic stainless steel grades by Shanghai No.1 steel plant is focused on the basic technology DDD, EAF, AOD, VOD and CCM, using hot metal in the EAF or AOD converter which has been treated in the Sumitomo DDD unit. This feature puts Shanghai No.1 in the first place in stainless steel production among plants applying such technology. The main production line DDD, EAF, AOD, VOD may vary depending on the temporary market conditions concerning the final product as well as on scrap and hot metal availability. In addition, this flexibility demonstrates the maintenance status of the equipment through production in the combination of DDD-AOD-VOD, EAF-VOD or in DDD-AOD only. The production range mainly includes the following steel grades:

Austenitic grades	**Ferritic grades**
AISI 304 and 304L	AISI 409. and 409L
AISI 316 and 316L	AISI 420
	AISI 430

Production process lines and technologies

The process routes set up by SMS Demag represents an innovative technology concept on the basis of hot metal and scrap which considers the local specific conditions of the steel plant and the high production capacity of the existing blast furnace. Replacing scrap by hot metal as virgin material not only reduces the concentration of tramp elements but also introduces a new source

of primary energy. The conventional EAF can be operated economically with up to 50% hot metal.
The availability of hot metal increases possible technological production alternatives. Bypassing the EAF allows direct production using the AOD converter or AOD converter and VOD plant without EAF operation. Duplex, triplex, EAF bypass, AOD bypass, production on scrap basis only can be applied depending on the actual production requirements as well the equipment maintenance schedule. Irrespective of availability of hot metal, the process line works in two typical configurations: duplex and triplex technology. Table 1 shows all possible technological combinations and flexibilities resulting from the installed equipment.
In recent years, technological developments in stainless steelmaking have focused on optimum solutions regarding available iron sources, raw material local conditions and energy. Especially steel plants where hot metal is available are seeking their chance in the production of stainless steel. Figures 2 and 3 show the technological solutions of Shanghai No. 1.
A blast furnace and an electric arc furnace with in-between DDD unit supply the AOD converter. The pre-metal obtained is a mixture of hot metal treated in the DDD unit (dephosphorization, desulphurization and desiliconization), molten scrap and ferrochrome and ferronickel in the EAF. As a converter charge, the metal constitutes approx. 80-90% of the converter's final weight.

Table 1. Shanghai No.1 Technological variants

Variant	DDD	EAF	AOD-L	VOD	Steel grade AISI	Remark
1	x	x	x		3xx, 4xx S xxxxx	Duplex , Hot Metal, Scrap
2	x	x	x	x	3xx, 3xxL 4xx, 4xxL S xxxxx	Triplex, Hot Metal, Scrap
3	x		x		4xx S xxxxx	EAF-By-pass, Hot Metal
4	x		x	x	4xx, 4xxL S xxxxx	EAF-By-pass, Hot Metal
5	x	x		x	3xx, 3xxL 4xx, 4xxL S xxxxx	AOD-By-pass, Hot Metal, Scrap
6		x	x		3xx, 4xx S xxxxx	Duplex , Scrap
7		x	x	x	3xx, 3xxL 4xx, 4xxL S xxxxx	Triplex, Scrap
8		x		x	3xx, 3xxL 4xx, 4xxL S xxxxx	AOD-By-pass, Scrap

Duplex and triplex technology

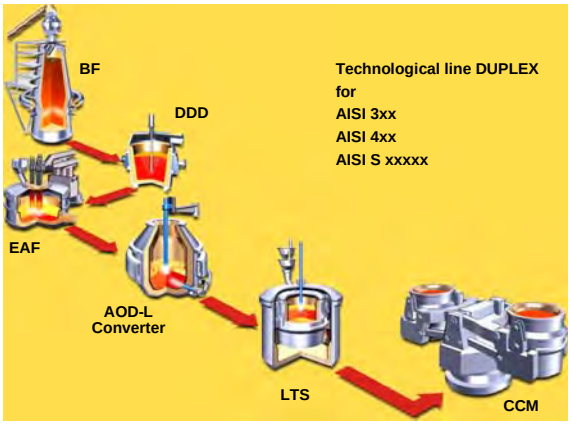

Figure 2. Duplex process

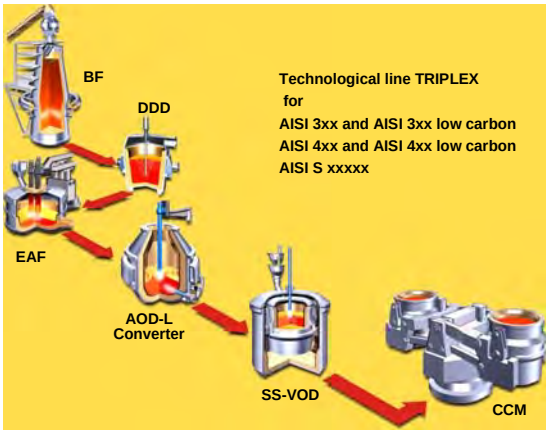

Figure 3. Triplex process

The remaining amount comes from alloy additions, mainly solid ferrochrome and ferronickel. The AOD process in the duplex technology allows the cost-effective production of steel grades with final standard carbon contents of more than / equal to 0.03%. Steel grades with a lower carbon requirement are produced by the triplex technology. In that case the AOD process is finished at a carbon content in the range 0.25-0.4%, which corresponds to a thermodynamic equilibrium through high Cr content (10-18%), a temperature of approx. 1,700°C and atmospheric pressure. Final refining of the AOD metal takes place in the SS-VOD plant.

EAF Bypass technology

Depending on the different commercial or operationally related situations prevailing in a steel plant, the production of stainless steel can be carried out by bypassing the EAF, Figure 4. However, the direct use of hot metal in the AOD supplies only part of the necessary energy. A relatively low temperature after the DDD treatment requires a corresponded temperature increase. This is attained by the specific control of oxidation reactions in the metal bath before charging of ferrochromium alloys. Due to the low hot metal energy input, the process is limited to the production of ferritic or duplex steel grades.

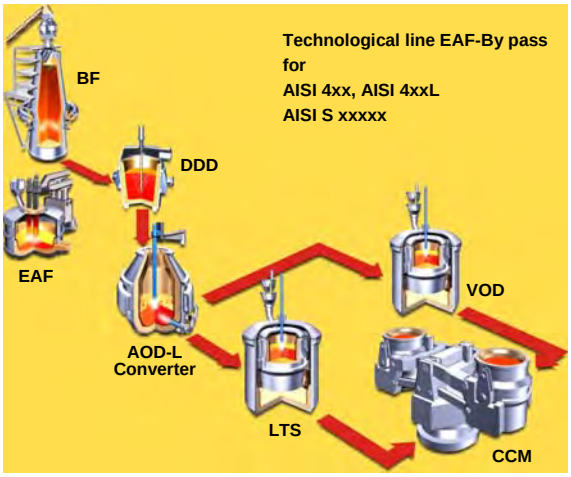

Figure 4. EAF Bypass technology

Steel plant equipment

Electric Arc Furnace

The new steel plant is equipped with an AC electric arc furnace which generally employs duplex and triplex technologies. Hot metal represents around 50% of the charge weight, with the furnace operating on one charging bucket. In the case of pure scrap heats, the final molten-metal weight requires the charging of 2 to 3 buckets. Different tapping weights are accomplished by technology applied. A tapped weight of 100t corresponds to the triplex and 120t to the duplex technology.
Large amounts of alloys and fluxes are introduced directly into the furnace via an automatic charging system.
Sophisticated process control is realized by supervisory system Level 1 and the process optimization system Level 2.
The main characteristics of the furnace are provided below.

Technical Data EAF

Type	AC EAF with spout
Tapping weight	100t (triplex) / 120t (duplex)

Transformer capacity	80 MVA
Primary voltage	35 KV
Secondary current, max	70 KA
Water-cooled sidewall panels and water-cooled roof	
Manipulator system	Oxygen flow rate 2500 Nm^3/h
	FeSi feeding rate 65-70 kg/min
	Carbon feeding rate 5-75 kg/min
Process and furnace operation	Level 1 and 2 automation systems

EAF performance figures for AISI 304 and stainless steel production

Power on time	≤ 45 min
Tap-to tap time	≤ 63 min
Electrical energy consumption	≤ 320 kWh/t_{steel}
Oxygen consumption	~ 10 Nm3/
Injection Carbon	2.6 kg/t_{steel}
Injection FeSi	2.2 kg/t_{stee}

AOD-L converter

Steel refining in a converter is an important link in the chain of interrelated production steps in the manufacturing and further processing of steel. The installed AOD-L converter is a complex system including a change vessel with submerged blowing tuyeres and an oxygen top lance. The AOD-L converter is equipped with 7 tuyeres which are protected all the time by shroud gas. Thanks the modern vessel exchange technique it is possible to replace a spent converter during in approx. 50 minutes. Due to the accelerated treatment time and reproducibility of the samples taken, the converter is equipped with a sub-lance system consisting of a sublance and an industrial robot.
All specific data of the converter operating in the steel plant are shown below:

Technical data AOD-L converter

Type	AOD-L converter with one-hole top lance and measuring sublance
Tapping weight	120t (triplex) / 135t (duplex)
Oxygen blowing rate	max. 250 Nm^3/min
Measuring sublance	metal sample and /or temperature
Plant, process and equipment control	L1, L2 and L3 automation systems

AOD-L converter performance figures for AISI 304 and stainless steel production

Refractory life time	≥ 70 heats
Tap-to-tap time	
Duplex with pre-metal carbon ≥3,5%	≤ 82 min
Triplex with pre-metal carbon ≥3,5%	≤ 65 min
Cr-yield	≥ 97%
Ni-yield	≥ 99%

VOD / LTS plant

The SS-VOD plant installed at Shanghai No.1 features a powerful vacuum system and strong bottom stirring through three porous plugs, thus ensuring excellent refining as well as mixing of the metal. The final carbon and nitrogen contents especially of ferritic steel grades can be reduced to 25 ppm carbon and to less than 60 ppm nitrogen. Extremely high vacuum pump

power, which allows producing a vacuum below 1 mbar and intensive metal stirring at a power of more than 1,300 W/t_{steel} at approx. 10 Nl/tmin, this plant can produce extremely clean steel with optimal properties suitable for direct casting within a reasonable short vacuum time.
The SS-VOD plant works as the third link in the triplex technology. With duplex technology the plant's function is reduced to supplying the right temperature and to chemistry adjustments of the metal refined in the AOD-L converter.

Technical data of SS-VOD / LTS plant

Type	SS-VOD / LTS
Tapping weight	120t
Process and equipment control	L1 and L2 automation systems

SS-VOD / LTS performance figures for AISI 304

Tap-to-tap time	≤ 65 min
Final carbon content	≤ 0.04%
Cr yield	≥ 98.5%
Ni yield	≥ 99%

Continuous Casting Machine

The continuous caster No. 3 is a vertical bending machine with one casting strand suitable for casting stainless steel grades. The usual casting thickness varies in the range of 180 to 200mm. The caster combines the advantages of the vertical and curve types and is used for producing slabs with maximum dimensions in the range of 1,600mm in width and 13.6m in length. Implemented into the stainless steel production line, this type of machine is identical to casters no. 1 and 2 also supplied by SMS Demag AG, which work on the carbon steel side. This situation not only allows easy maintenance and spare parts handling but also offers high flexibility and optimal utilization of the load factor for both caster lines.

Technical data of CCM

Type	stainless steel caster, vertical bending
Tundish capacity	26.2t
Strands	1
Caster radius8,636mm	
Max. casting speed	1.6 m/min (austenitic SSt 200 mm thick)
Oscillation frequency	60-360 c/min
No. of segments	9
Process and equipment control	L1 and L2 automation systems
Max. sequence length	6

THE EXTENSION OF OUTOKUMPU STECKEL MILL AND ITS EFFECT ON THE QUALITY OF THE HOT ROLLED MATERIAL

P. Saxlund, A. Nuortio, M. Niska, E. Puukko

Tornio Research Centre, Outokumpu Tornio Works, Finland

Abstract

In the end of April 2002 Outokumpu (Avesta Polarit) made an investment decision to increase the production of its Steckel mill from the level of 1 million ton to 1.7 million ton of stainless steel. To attain this drastic increase in production, it was the first time in the history that three additional finishing stands were installed after an exit-side of the Steckel furnace. Laminar cooling was renewed and a new level 2 automation system was installed. It was specially designed for this particular configuration and included pass schedule model and profile, contour and flatness model for calculation of set-up values for the whole mill line. Also the existing level 1 system was extended accordingly using most modern technology.

This paper gives an overview how the quality was affected by the installation of the new equipment and the modernisation of the automation. The main parameters to characterise surface quality are compared. The data mining techniques are used to analyze change in the cross-thickness profile and flatness of the hot coil. The evaluation of the strength gives an example how the data from the further process is utilized.

The defect frequency of the “rolled-in-scale” decreased down to fifth after the modernisation. With the new mill configuration and control system better thickness profile with less variation was achieved than before. The flatness was improved to meet up high requirements of further processing in the RAP-line. The strength of the hot rolled material was kept at the previous level.

Project phase and final installation

In the end of April 2002 Outokumpu made an investment decision to increase the hot rolling mill capacity up to 1.7 million ton. According to the time-schedule, the start up of new capacity would be after the annual maintenance shut down in the beginning of September 2004. Other targets were to disturb production as less as possible, because the investment was installed into the ongoing mill line, and also to increase the maximum product weight from 26 to 30 ton.

In the feasibility studies it had been found that the best solution was to implement three additional stands after the Steckel mill. Final procedure of implementation was not yet been decided, but enough information was already available. The old walking beam furnace had also to be modernized for the new maximum weight and repaired by using gathered experience and new technology. Also numerous other equipments and investments were necessary as a consequence of this size of extension. For example, the old table based model was planned to be replaced by the most modern and adaptive model for the whole line. As an automation concept this combination line was the first in the world. The Steckel mill could do reversing passes and in the final pass it would be one of the stands in the finishing train. For better looper control, a

pinch roll was located between the Steckel furnace and the first additional stand and the first looper between the pinch roll and the first stand. For better quality and quality control it was installed a multi-channel measuring device after the last stand and automatic surface inspection in front of the down coiler. An accurate control of coiling temperature was enabled with a new laminar cooling unit after the rolling. Flow sheet after the extension is shown in Figure 1, the new facilities circled with dashed lines.

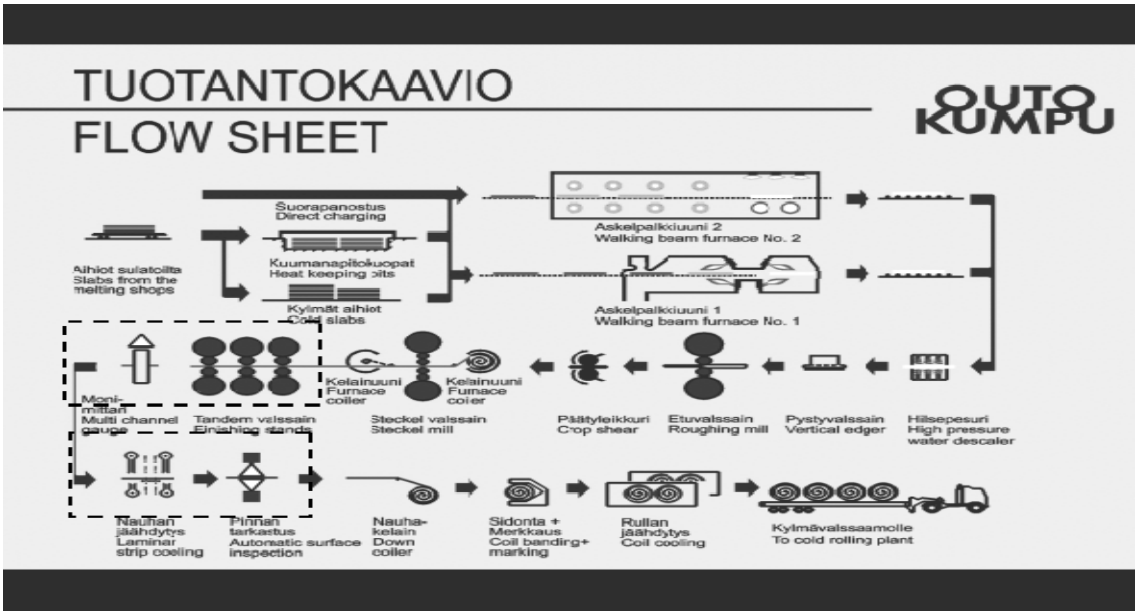

Figure 1. Flow sheef of the hot mill after the extensions.

Reliability was achieved by mechanical, electrical and automation by the end of the year 2004, and finally during March 2005 the whole system was ready to a half-year test run period, when reliability and performances were tested. Final acceptances of supplies were made in October 2005.

The process of a combined Steckel- and tandem-line is quite challenging due to a fast and big temperature change in the top and tail part of the strip.[1]That causes much higher demands for control and accuracy of set-up models than the conventional hot strip mill process, but as an extension of Steckel-mill it was very reasonable by the cost-wise, while aforesaid conditions are valid.

Cross-thickness profile

Compared to the 4-high tandem mill a 6-high steckel mill is more efficient in controlling the profile due to the intermediate rolls that can be shifted and bended. On the other hand, CVC-type work rolls that are used in the 4-high stands enable a wider control range of profile than rectangural work rolls. In addition the set-up model for profile and flatness, calculations have an important role when targeting to a homogenous convex profile shape. For example, wih the aid of roll contour calculation the roll wear can be taken into consideration when planning optimal shifting schedules of work rolls.

The evaluation method and results

The classification method based on the Kohonen network can be utilized to identify all profile shapes of the hot strip.[2]The results of the classifications are visualized in the 2-dimensional maps that significantly helps to draw conclusions. Using this method, the development of total profile

shape can be evaluated, as shown in Figure 2.On the left side all classified half-profile types are presented by relative crown-values. The problematic profile shapes from further processing point of view are marked by a question mark.The fraction of every profile type is presented at the rigth side before and after the extension with the Steckel mill and with the Steckel-tandem configuration.

It can be seen that the profile shape is clearly better controlled with the Steckel-tandem combination. The profile shape is mainly convex having more or less edge drop. Irregular convex and very deep shapes have 10% fraction only. The total fraction of problematic profiles shapes was decreased from 50% to 10% even if the set-up models were not yet finally tuned at the time of data analysis.

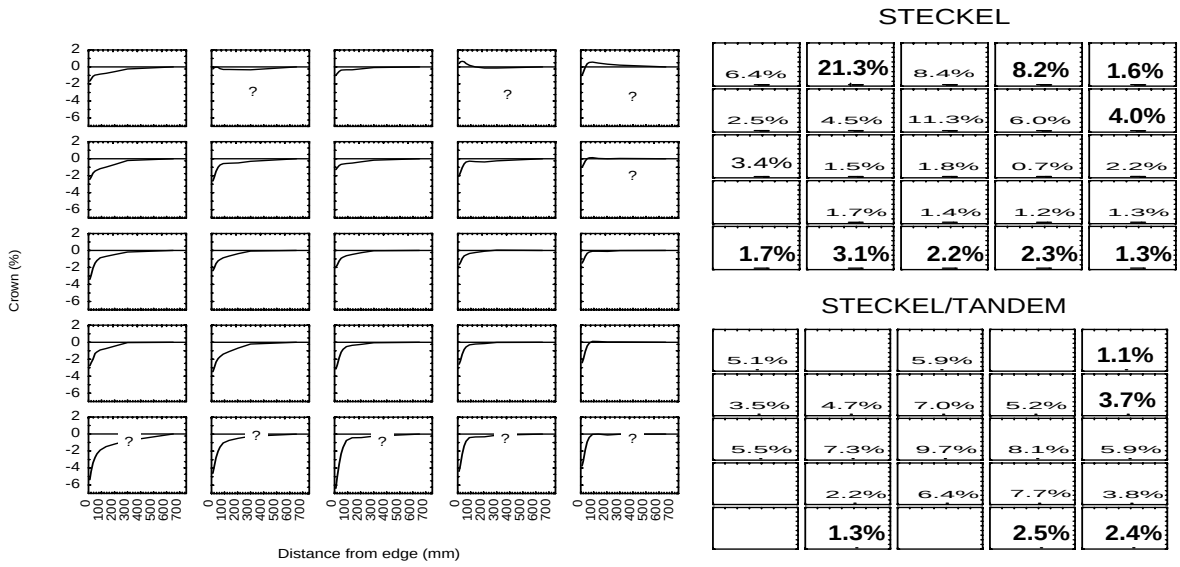

Figure 2. The comparison of profile control between the Steckel and the Steckel-tandem mill.

Flatness evaluation

If all flatness measurements for one coil are drawn in the same graph, a measurement series that resembles the one in Figure 3a is obtained. In this study, information on black coil flatness characteristics was extracted from tensionmeter data by fitting a polynomial curve to each flatness measurement. The method which was presented in Ref. [3], implies fitting a second order polynomial function to each flatness measurement by the least squares method, and then determining the flatness class on the basis of the coefficients of the polynome.

$y(x) = a_0 + a_1 \cdot x + a_2 \cdot x^2$, where x is the distance from strip center line (1)

The sign of the parameter a_2 indicates which of the following flatness classes describes the strip flatness more accurately: “long center” or “long edges”. The absolute value of the parameter a_2 describes the magnitude (degree of severity) of the flatness defect in question. The following rules of thumb apply:

a1<0 → “serpentinity”, right hand side of the strip is longer than left hand side,
a1>0 → “serpentinity”, left hand side of the strip is longer than right hand side
a2>0 → strip has long center
a2<0 → strip has long edges.

When one strip passes the stressometer, a flatness “path” or “trajectory” is generated which describes the development of flatness from tail end to head end for that particular coil. When a large number of coils is studied, each coil will be related to a list of parameter values, or simply a “flatness vector”. These lists of parameter values can, in turn, be classified by any common classification method, such as neural network classification. Thus, the data obtained from the polynomial fit analysis, was prepared for second stage analysis where a self organizing map was used for classification. In Figure 3b the result of the two-stage analysis approach is shown; the most common flatness defect development types in the longitudinal direction of the strip are identified for a batch of coils.

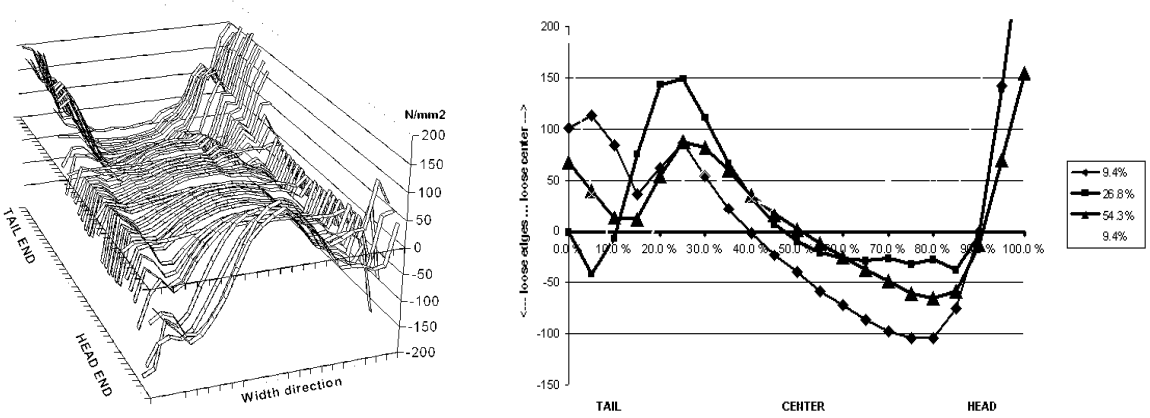

Figures 3a and 3b. A typical flatness measurement (a) and four most common flatness classes found in the data (b).

By comparing the typical flatness trajectories between two sets of data representing different laminar flow cooling strategies, it could be found out that increased laminar flow cooling resulted in a better flatness. This observation was proven to be valid specially in the case that the coils were soaked to water pool after hot rolling.

Strength evaluation

The material strength was estimated on the basis of rolling forces in the 3-stand black coil cold rolling process. The basic philosophy was: “the higher rolling force you use on a workpiece to reach a certain reduction or the more tensions you use on that workpiece, the harder must the material be”. Namely, deformation by rolling force and deformation by tension are alternative ways of achieving deformation. A simplistic model describing this phenomena was found in Grundlagen des Bandwalzens [4].

Deformation resistance k_{fm} was calculated in each stand and a simple deformation resistance curve function was fitted with the three obtained points. From this calculated curve it was read how much resistance the material generates against 25% reduction. Strength was estimated at every measurement points along the strip length as shown in Figure 4a. As a result of this procedure a “strength vector” could be assigned to each coil in the study. Because hundreds of coils were analysed, a data set was generated upon which common statistical analysis could be performed. In Figure 4b averaging and calculating limits of standard deviation is done, in order to compare the strength before and after the change in laminar flow cooling. The increased laminar flow cooling and more rapid pass through time in the Steckel-Tandem mode did not seem to have a significant effect on material yield strength.

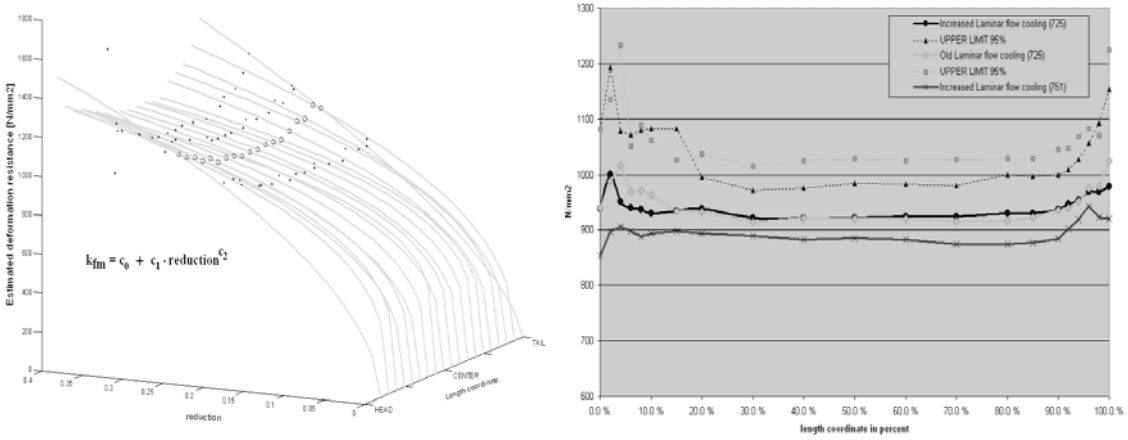

Figures 4a and 4b. Illustration of the exponential-fit method (a) and the result of the material strength analysis (b).

Influence of Hot Rolling Practice on Surface Properties

After installing of additional stands behind the Steckel mill some positive signals regarding the surface properties were observed. In the following chapters influence on re-pickling rate and on thickness of oxide scale layer are dealth with.

Re-Pickling Rate of Hot Rolled AISI 3XX Material

During the Steckel hot rolling practice the re-pickling ratio of hot rolled AISI 3xx material caused by rolled in scale –defect varied annually between 1.2-1.9% (see Figure 5). Higher surface roughness values were typically detected within areas affected by rolled in scale –defect.[5]Rough areas were typically seen visually as small ruptures transverse to the rolling direction. After installing of additional stands, the re-pickling ratio decreased to the level 0.3-0.5% (Figure 5). This advantageous result could possibly be caused by the feature, in which three tandem rolling stands are falling roughness peaks of rolled coil always in the same direction while the steckel mill typically falls peaks in opposite directions during sequential rolling passes.

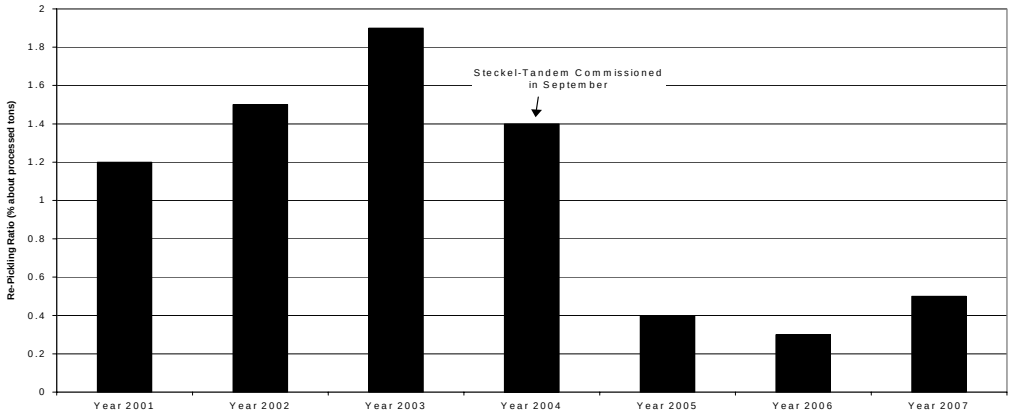

Figure 5. Re-pickling ratio of hot rolled AISI 3XX material due to by rolled in scale –defects.

Thickness of Oxide Scale for Black Hot Rolled AISI 304 Material

In Figure 6 is presented thickness values for oxide scale layer measured with the eddy current method at the center length of coils. Measuring points were located at three areas (¼-, center- and ¾-width) along the width direction. According to Figure 6 thickness values between 54 and 58 µm were measured after Steckel rolling but only about 20 µm after Steckel-Tandem rolling for 3.5 mm coils. For 6 mm coils, the corresponding values are seen to vary between 65 and 71 µm after Steckel rolling and settle between 42-47 µm after Steckel-Tandem rolling.

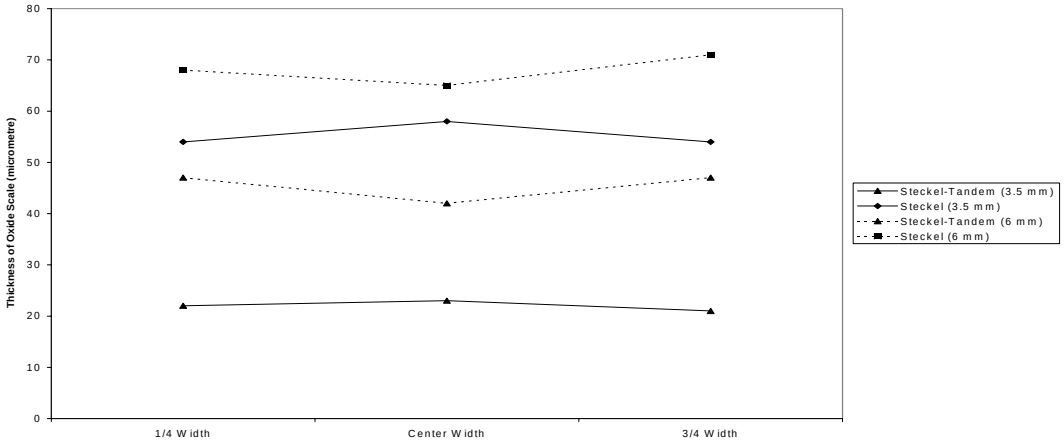

Figure 6. Thickness profile of the oxide scale for black hot rolled AISI 304 coils (measured at the center length of coils).

Conclusions

By the aid of data mining techniques it could be concluded that the total fraction of problematic profile shapes decreased from 50% to 10%, when the hot rolling process was extended to contain the 3-stand tandem.

A more intense laminar flow cooling strategy was chosen in order to minimize the formation of severe loose edges in the water pool cooling process. The increased power of laminar flow cooling due to the Steckel-Tandem mode did not seem to affect the material strength.

After installing the additional Tandem stands, the re-pickling ratio for hot rolled AISI 3XX material caused by rolled in scale –defect was observed to decrease down to fifth. Due to additional stands, the thickness of oxide scale on AISI 304 material was measured to be typically some tens of micrometres smaller than after Steckel rolling.

References

[1] P. Saxlund: “Extension of Outokumpu Steckel mill”, METEC InSteelCon 2007, Duesseldorf, 2007.

[2] E. Puukko, “The recognition of the regular and the irregular strip profiles and shapes”, Steel Rolling 2006, Paris, 2006.

[3] A. Nuortio,“Tutkimus koskien kuumanauhojen tasomaisuusprofiilia “, POHTO Seminar Metallurgisten prosessien muuttujien korrelaatiot, Oulu, 2004

[4] K. Weber: “Grundlagen des Bandwalzens”, 1973, p. 48

[5] M. Niska, M. Prakkula: AvestaPolarit Stainless Internal Report 5397-5381/02, Tornio, 2002.

STATUS OF AUTOMATED SURFACE AND QUALITY INSPECTION IN OUTOKUMPU TORNIO WORKS

P.T. Mure

Tornio Cold Rolling Plant, Outokumpu Tornio Works, Finland

Overview to Outokumpu and Outokumpu Tornio Works

Outokumpu is an international stainless steel company, which operates in some 30 countries and employs 8000 people. Outokumpu Tornio Works is located in Tornio, Finland, being the largest production unit of the company. The mill is located by the harbour and the Baltic Sea. Between 2001 and 2004 Outokumpu invested heavily for doubling the production capacity in Tornio. The current production capacity is double compared to the figures in year 2000. As the production levels shot up so drastically, it was evident that Outokumpu had to invest into quality and surface inspection. Former, purely manual, practices in maintaining the high quality levels of steel were not applicable in the new, totally changed production environment.

Surface Inspection at Tornio Works

To guarantee high quality of stainless steel sheets and coils they are inspected in various phases of the production chain. Obviously, the quality inspection includes many activities and not only surface inspection. Nevertheless, this paper focuses on surface inspection. As an example, melt shop quality means many chemical analysis checks and of course, highly controlled production process and accurate raw material selection.

First surface inspection takes place at Hot Rolling Mill. Inspection is done by surface inspection system (SIS) and manual inspector is acting only as a system administrator once a week. Inspector's role is to develop and tune the inspection system operation according the current needs.

Second inspection is done after the primary annealing and pickling of black hot rolled coil. This takes place at cold rolling plant. In this inspection the strip edges and surface are inspected and evaluated and so called Hot strip evaluation is carried out. The inspector gives a six level grading to the coil, this grade affects coil production route and possible corrective actions.

Normally the coil gets quality class 1 or 2 in Hot strip evaluation and continues to cold rolling. After the cold rolling the coil normally continues to final annealing and pickling (AP) of the strip. Also an intermediate AP-round between two cold rolling process is possible but avoided.

Cold strip inspection and evaluation is performed after the final AP-process. This is the most important inspection during the process and third inspection during the cold rolled strip processing. In cold strip inspection possible strip surface defects are monitored and coded into the system. These systems are a production control system RETU or a quality monitoring system PIHA. Strip thickness and width are also measured and recorded into the systems. In this inspection the inspector makes some special notes if there is something exceptional in the strip

quality. For example, this note may contain information of the defect appearance and of its exact location.

The special feature in the cold strip inspection is the applicability evaluation (schematic presentation of applicability evaluation is presented in figure 1). In this process the inspector makes certain that the strip is suitable for the customer and forwards the strip into following processes (skin pass mill, grinding, brushing). Of course, if the strip quality is not applicable to the customer, strip is transferred to so called sidetrack, which is a hold-status for the strip movement. Sidetrack means that quality specialists will consider in more detail which kind of corrective actions should take place to fulfil the needs. For example, if the strip has flatness defects, there will be an additional process in tension levelling line.

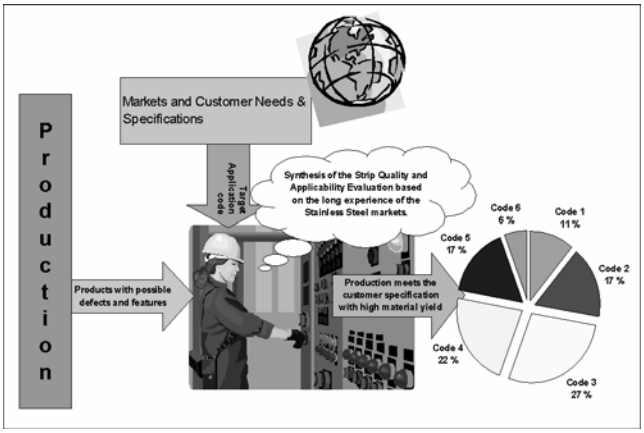

Figure 1. Schematic presentation of the third surface inspection for the cold rolled products and applicability evaluation of the strip.

The final and fourth quality check happens in finishing lines where inspector takes care that only customer specified material will be cut into coils and sheets. At finishing lines the inspector is also a member of line production team and takes care of all customer-related tasks during the shift. For example, these tasks include marking the packing/shipment codes, scrapping of the off-gauge material and as well scrapping of the defected material at the strip head and tail.

As said, in total the surface inspection at Outokumpu Tornio Works includes four different steps. All major phases in surface inspection regime can be seen from the following flow chart (Figure 2).

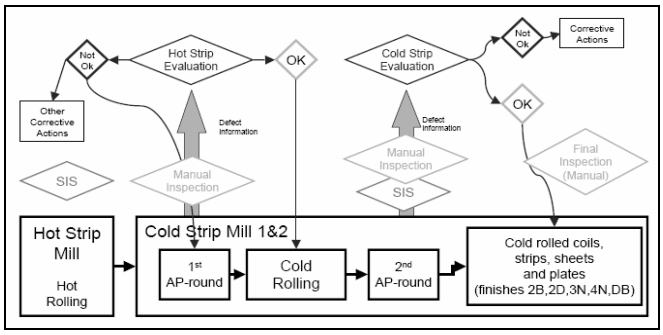

Figure 2. Surface inspection at Tornio Works

Machine Based Surface Inspection at Tornio Works

Outokumpu has four different SIS's installed into production lines at Tornio Works. One is at Hot Rolling Mill while others are at Cold Rolling Plants 1 & 2. More precisely the systems at

Cold Rolling Plants are located at annealing and pickling line 4 (AP4) and RAP5-line. AP4 is one of the final annealing & pickling lines of cold rolled (2B) products at Tornio Works. RAP5 is a line combining Rolling, Annealing and Pickling processes. There is also a Skin Pass Mill at the end of the RAP5-line, which means that the line includes all necessary steps to produce finish 2B material to markets.

As said in the preceding chapter and seen in Figure 2, the surface inspection machines are inspecting the product in different processes and also their inspection phase is different. The hot rolling mill system is doing the first phase inspection and role of the system is more or less controlling, not a statistical role as normally surface inspection has. The system has a rather unique feature that if the system notes a serious roll marks or defects coming from the tandem hot rolling mill, the system gives an on-line alarm to tandem mill operator as well as to down coiler operator. Also, the inspection system shows automatically to operator which defect was alarming and gives a quick opportunity to decide whether the rolling should be stopped or not. If yes, the operator will check the work rolls and continue rolling. If not, operator may follow the development of the alarming defect and stop the production later.

In this regard the AP4 system is doing traditional surface inspection after the final cold rolling and final AP-process (inspection phase 3). At the moment system is accepted and fine-tuning for the statistical role is going on. This is explained in more detail in following chapters.

RAP5 inspection systems (one at the exit of the line and another after the tandem cold rolling mill) are a complicated combination of both of the preceding roles. The SIS after the tandem cold rolling mill (TCM) is planned to have a much similar role than hot rolling mill SIS has. This means that the system is planned to give an immediate and enough reliable online alarm to TCM-operator to report if there is a serious defect at the strip surface. Then corrective actions (especially work roll change) could be done according the measured need. As well, this way the amount of defected material is minimised.

The SIS at the exit of the RAP5 is acting more traditionally in inspection phase three. Most significant difference to AP4 SIS and third phase inspection is that the RAP5 exit system is not only inspecting the cold rolled material in 2B finish but also hot rolled material and RAP5 special finishes as RAPTM2E. This specialty in inspection is due to unique material flow at RAP5 when different processes can be carried out at the same line. Nevertheless, despite of these differences the exit SIS is a main tool for the line inspector and is reporting of the strip defects to PIHA-system. As well as with AP4-system, the future development of the system is explained in following.

Current Status of the Machine Inspection at Tornio Works

The AP4 system is fully accepted by Outokumpu. RAP5 exit is under performance tests and presumably will be accepted by the time this paper is published. It is obvious due to a fact that at the moment (January 2008) results are already good or even very good for all tested steel finishes. Similar performance tests of the RAP5 tandem-SIS will start soon after finishing the ongoing tests of the Exit-system. Hot Rolling mill SIS is still under development phase. New cameras were installed into the system to improve the detection of edge cracks and some other edge defects.

Performance tests of Surface Inspection Systems

In order to obtain a reliable understanding of the system performance, Outokumpu developed with the SIS supplier ABB a two-phase testing method. Firstly the system capability to detect

strip surface defects was tested. Second phase of the performance test was to reveal the systems ability to classify the defects into different defect classes. In ABB system defect classification performance also means the ability of the system to tell the defect severity.

It is important to carry out the performance tests respectively. This is because the detection test tells a SIS user whether the system is really seeing an entire defect profile of the strip or not. If not, the SIS user would only have a partial view on strip defects and possibly some type of defects were not detected at all. Hence, similarly the classification test would only be partial. On the contrary, if the detection performance test clearly tells a SIS user that the system is seeing all or enough of the relevant defects, then the classification test is relevant and easy to do.

More theoretical view to detection performance is given in the Figure 3 and Figure 4. In Figure 3 all three logical sets of defects and detections are shown. First and obvious set is including all defects of the strip. It is called set A. Current and former practices in manual inspection have given a reliable proof that a skilled human inspector is collecting a descriptive set of the strip defects. This set is called set B and normally it is not equal to set A. An additional typical feature for this set is that it only includes actual defects and, hence, it is a true subset of set A. Third logical set is phenomena detected by the surface inspection system, this set is called set C.

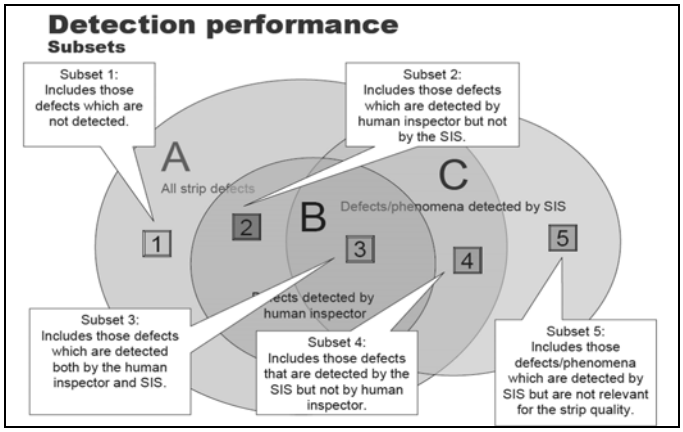

Figure 3. Sets and Subsets in Detection Performance

Target for the performance testing is presented in Figure 4. It is obvious that system should be able to detect all defects that the human inspector is seeing or detecting. More theoretically this means that subset 2 will be equal to zero and subset 3 is a real subset of set C. In addition, when targeted to a maximum performance of the system, subset 4 should be maximised. On the contrary, subset 5 should be minimised to avoid so called pseudo detections.

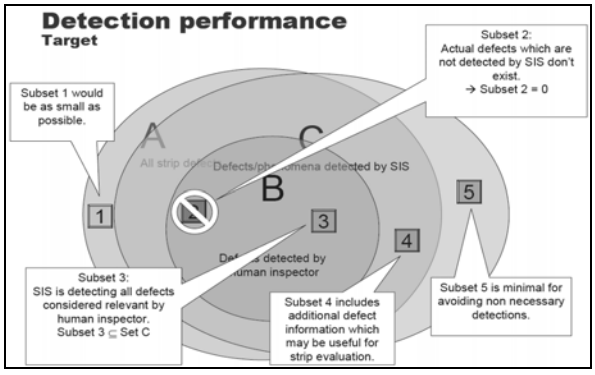

Figure 4. Target of SIS Detection Performance

Future Development of the Machine Based Surface Inspection

The performance tests of the AP4-system clearly told that it was possible to get a satisfactory system performance, i.e. the system was detecting all relevant defects (see Figure 4). What was also discovered was that a huge amount of other, not so important but still visible, defects were detected. This means in the terms presented of the figures above that subset 2 was rather small if not even zero and there also existed a rather large subset 4. Hence, it was evident that a surface inspection system would bring more information on the strip surface quality than the traditional manual methods did. Similar performance tests at RAP5 confirmed this.

If the surface inspection system has a role like Hot Rolling Mill or RAP5-Tandem systems have, it is rather simple, at least in principle, to solve the problem of sensitive defect detection. In this kind of an application, relevant defects are separated from the mass of detections by defect classification and only the most relevant ones are shown on the system screen. Others, like smaller defects, are discarded based on the same classification and not shown on the screen. Of course, there are also some difficult and complex cases but still the main principle in this kind of a case remains simple.

On the contrary, if the SIS role is in cold strip inspection and applicability evaluation, the simplicity disappears. Existing rules of applicability evaluation were not directly applicable to SIS data for a couple of major reasons. Firstly, the format of the data is different from that the older RETU-production system has. Secondly, the system is seeing not only the set B defects, but also a large number of defects belonging to subset 4. Also some pseudo detections exist. Thirdly, the defect classification has some uncertainty with unusual or rare defects. And finally, the existing rules for the applicability evaluation were more or less verbal, not a machine compatible and enough exact numerical rule hierarchy.

In order to solve these problems and also update current practices, a theoretical approach to a problem was created. The surface inspection process was divided into logical steps and each step will be solved separately. Then those basic steps will be fitted together. Basic schematic equation of the partial division principle can be seen in Equation (1) below:

$$f(x) = \underbrace{\begin{pmatrix} a_{11} & a_{12} & a_{13} & a_{14} & a_{15} & a_{16} \\ a_{11} & & & & & a_{26} \\ a_{11} & & & & & a_{36} \\ & & & & & \\ & & & & & \\ a_{i-3,1} & & & & & a_{i-3,6} \\ a_{i-2,6} & & & & & a_{i-2,6} \\ a_{i-1,6} & & & & & a_{i-1,6} \\ a_{i,6} & & & & & a_{i,6} \end{pmatrix}}_{A_{i,6}} + B_{i,6} + C_{i,6} + \ldots + K_{i,6} = y \qquad (1)$$

in which

matrices A…K are including possible main features of SIS inspection.

- Matrix A is a set of basic rules affecting applicability of the strip. These rules tell the maximum surface defect severity, which is tolerated in a relevant applicability class. Matrix A includes as many columns as there are applicability classes. On the other hand, number of rows i is equal to the number of the defect classes affecting applicability.
- Matrix B includes the SIS dependent weight factors, i.e. the sensitivity factor. This means the defect detection sensitivity factor for each defect class (for a skilled human this is about 0). Matrix B must be defined separately for each of the surface inspection systems.

- Matrix C includes classification performance factors, i.e. the classification correctness. As well, this is a SIS dependant factor and must be defined separately for each of the surface inspection systems. For a skilled human inspector this is » 0, depending about person.
- Matrices further to K are containing other, still unexplored factors.

Matrices A and C have been determined by Outokumpu. Next step will be to determine matrix B, the sensitivity factor. As said, it is a system variant and depends on the SIS settings and material in inspection. Probable tool for solving matrix B is a numerical approximation, main input for this is a comparison between strip applicability evaluation made by human inspector and a SIS output after calculating Equation 1.

Benefits for above mentioned development are 1) higher accuracy of the applicability evaluation, 2) easier evolution of the rule library (matrix A) in case of changes in customers' needs and 3) improved material flow and yield due to the more accurate applicability evaluation of cold rolled material.

Conclusions

Outokumpu Tornio Works is a highly integrated steel mill producing stainless steel. Demand for surface quality is obviously high for such a high valued product. Due to this fact, a quality and surface inspection is carried out with similarly high standards.

Surface inspection regime covers all crucial steps in the production chain. Role of the inspection changes from a purely controlling inspection (in early steps) to a statistical quality inspection (at the end of the production chain). Needs for the inspection changes as well.

Traditionally, the surface inspection has been done by human inspectors. This era of pure manual inspection is coming to its end due to installation of surface inspection systems to new production lines. Also the older lines are equipped with such systems. Hence, practices of surface inspection must as well be evolved. Aim of the surface inspection systems is to assist and improve the quality of surface inspection. In more concrete terms this means that the accuracy and coverage of inspection will be improved. Unfortunately, there may be some, still unexploited, problems as well.

Outokumpu Tornio Works has already a rather good experience of surface inspection systems and their abilities. At the moment, systems are fine-tuned into production and cold strip surface inspection. One, rather obvious, short-term goal is to get such inspection results from machine inspection that former manual and future machine based surface statistics are comparable to each other and have the same reliability. Basic measures for realising this are ready and only wait for implementation.

THE USE OF FLAMELESS OXYFUEL IN STAINLESS STEEL PRODUCTION

T. Niemi[1], O. Ritzen[2], J. V. Schéele[3]

[1]Oy AGA Ab, Finland, [2]AGA UTAB, Sweden, [3]Linde AG, Germany

Abstract

Increased throughput and flexibility, reduced fuel consumption and decreased emissions (e.g. much less CO_2 and NO_X) are the main reasons the use of oxyfuel based melting and heating become increasingly popular.

New demands and challenges from the industry have been met by a continuous development work. As a result, in parallel to the conventional oxyfuel there are today established very interesting technologies. Among those, one of the most important ones seems to be flameless oxyfuel combustion. This new technology has been proven to deliver astonishing results.

In stainless steel production, the first installations of flameless oxyfuel took place in 2003 at Outokumpu's operations in Sweden. Today flameless oxyfuel is applied in drying and preheating of ladles and AOD converters, and for heating in reheat furnaces and annealing lines. It provides excellent temperature uniformity and reduced NO_X emissions at the different types of installations at companies like Acerinox, Outokumpu and Sandvik.

The paper describes the state-of-the-art of flameless oxyfuel, including results from installations in preheating of ladles and AOD converters, and from heating in reheat furnaces and annealing lines. Typical results are increased throughput capacity, decreased fuel consumption, and substantially lowered emissions of CO_2 and NO_X.

Introduction

Heating and melting with oxyfuel have been used in the steel industry for decades, however, mainly in the areas of scrap melting and vessel preheating. Among stainless steel producers this use has been more restricted.

Prompted by rapidly rising fuel prices in the 1970s, ways of reducing fuel consumption in reheat and annealing furnaces were first considered. This laid the foundation for a development that led to the use of the oxyfuel solutions also in rolling mills and forge shops. In the middle of the 1980s AGA began to equip the first furnaces with oxygen-enrichment systems. These systems increased the oxygen content of the combustion air to 23-24%. The results were encouraging: fuel consumption was reduced and the output (in terms of tonnes per hour) increased. In 1990 AGA converted the first furnace to operation with 100% oxygen, i.e. full oxyfuel combustion. For the past 15 years AGA (Member of The Linde Group) has been pioneering the use of oxyfuel in this field.

As of today, Linde has made more than 110 furnace installations of its REBOX® oxyfuel solutions in reheating and annealing. With in-house furnace and process engineering experts, Linde has the proven capability to deliver turnkey projects with short implementation time and guaranteed performance.

From conventional oxyfuel to flameless oxyfuel combustion

In an air-fuel burner the burner flame contains nitrogen from the combustion air. A significant amount of the fuel energy is used to heat up this nitrogen. The hot nitrogen leaves through the stack, creating energy losses. When avoiding the nitrogen ballast, by the use of industrial grade oxygen, then not only is the combustion itself more efficient but also the heat transfer.[1]

Oxyfuel combustion influences the combustion process in a number of ways. The first obvious result is the increase in thermal efficiency due to the reduced exhaust gas volume, a result that is fundamental and valid for all types of oxyfuel burners (Figure 1). The next result is that the concentration of the highly radiating products of combustion, CO_2 and H_2O, is increased in the furnace atmosphere. For melting and heating furnace operations these two factors lead to a higher melt or heating rate, fuel savings, lower CO_2 emissions and – if the fuel contains sulphur – lower SO_2 emissions. Oxyfuel combustion allows all installation pipes and flow trains to be compact without any need for recuperative or regenerative heat recovery solutions. Combustion air-blowers and related low frequent noise problems are avoided.

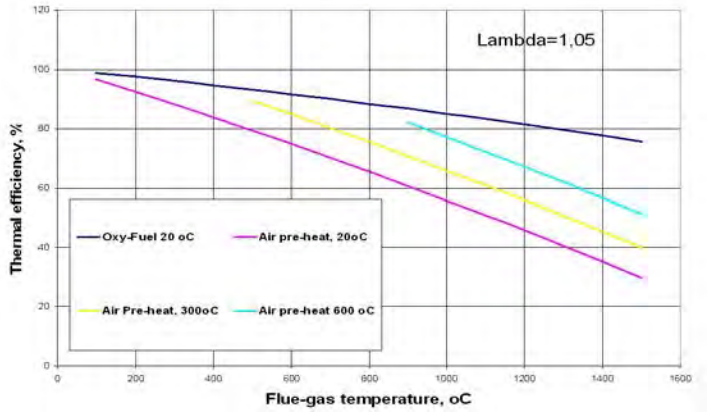

Figure 1. Comparison of overall thermal efficiency when using airfuel and oxyfuel.

Two features of oxyfuel combustion process need to be addressed: the increase in flame temperature and the subsequent potential of forming thermal NO_X. It is important to note that NO_X formation is highly dependent on the design of the oxyfuel burner, furnace specifics and the process control system. In fact, oxyfuel combustion has been used for many years to reduce NO_X emissions to meet environmental regulations.

Lowering of NO_X emissions

The legislation relating to NO_X emissions is strict, and permissible emission levels are constantly being reduced. It is worth noting that nitrous oxide, in addition to having many well-known adverse effects, is also one of the greenhouse gases listed in the Kyoto Protocol; its so-called global-warming potential is 230 times that of CO_2. Bearing this in mind, development work started in collaboration with customers to find even more effective oxyfuel solutions.

Three things control the formation of thermal NO_X: partial pressure of oxygen; partial pressure of nitrogen; combustion temperature, i.e. NO_X formation temperature. For each of these prerequisites there are different measures that can be undertaken to minimise the formation of

NO_X. Thus it is possible to formulate a strategy, including – for each of the items – the following measures:

- Partial pressure of oxygen
  - Ensure a well-functioning combustion and control system
  - Minimise air ingress by means of tightness and strict control of the furnace pressure
- Partial pressure of nitrogen
  - Avoid having nitrogen present in the oxidation media
  - Minimise air ingress by means of tightness and strict control of the furnace pressure
- Combustion temperature
  - Flameless combustion

Although only oxygen is used in the conventional oxyfuel combustion process, nitric oxide is produced as a result of the high flame temperature and the ingress air. To lower the peak temperature and improve the flame conditions, the introduction of so-called staged combustion was an important first step to achieve reduced NO_X emissions. However, due to authorities' continuously lower emission permit levels, further technical developments had to be taken on.

Flameless oxyfuel – faster and more uniform heating with ultra low NO_X

As mentioned, a key parameter in achieving low NO_X is reduction of flame temperature. Below a temperature of approximately 1,400°C NO_X formation is limited, but above this temperature a dramatic increase in NO_X occurs (Figure 2). Conventional oxyfuel combustion can exhibit flame regions with temperatures above 2,000°C. One way of reducing the flame temperature is to use the principle of 'flameless combustion'. This principle has been known for many years but has only recently been exploited industrially.

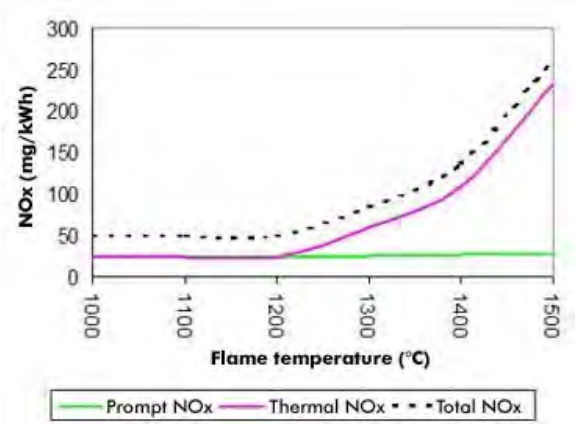

Figure 2. NO_X formation in relation to the flame temperature.[2]

The expression 'flameless combustion' rather expresses the visual aspect of the combustion type, i.e. the flame is no longer seen or easily detected by the human eye. Another description might be that combustion is 'extended' in time and space – it is spread out in a large volume. This is why it is sometimes referred to as 'volume combustion'. Such a flame has a uniform and lower temperature (Figure 3).

There are two main ways of obtaining the flameless oxyfuel combustion mode: either dilution of the flame by recirculating part of its flue gas to the burner, or use of separated injection of fuel and oxygen at high velocities. The mixture of fuel and oxidant reacts uniformly through flame volume, with the rate controlled by partial pressures of reactants and their temperature.

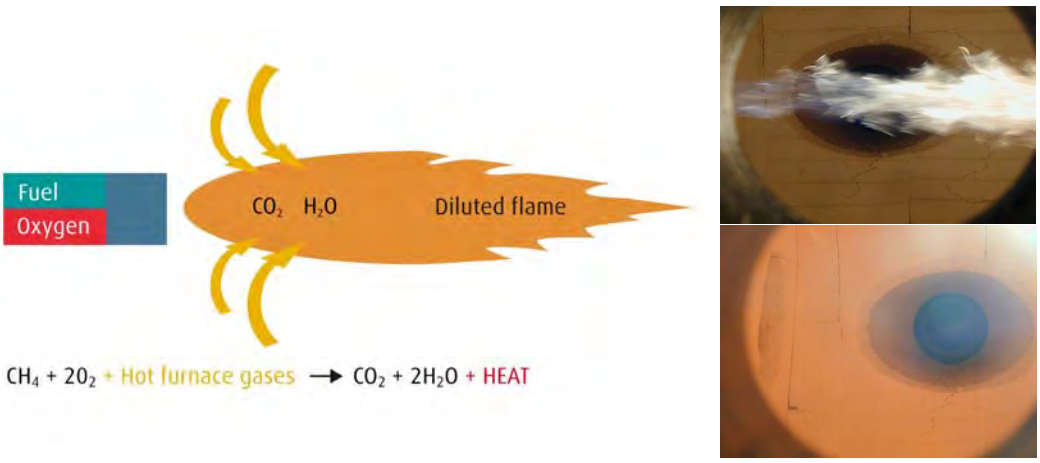

Figure 3. In flameless oxyfuel combustion the flame is diluted by the hot furnace gases. This reduces the flame temperature to avoid creation of thermal NO_X and to achieve more homogenous heating of the steel. The top-right photo shows the hot oxyfuel flame coming from the burner on the left. The bottom photo shows flameless combustion – a diluted and almost transparent flame.

In addition to reducing the temperature of the flame, flameless oxyfuel burners effectively disperse the combustion gases throughout the furnace, ensuring more effective and uniform heating of the material – the dispersed flame still contains the same amount of energy but is spread over a greater volume – with a limited number of burners installed.

With the low flame temperatures of flameless oxyfuel, formation of thermal NO_X is avoided.This was confirmed in an investigation carried out by the Royal Institute of Technology in Stockholm, Sweden.[3] Trials in pilot-scale furnace showed that even with large volumes of ingress air entering the furnace NO_X levels remained low (Figure 4). This is a typical problem for old and continuous type of furnaces. Conventional oxyfuel and regenerative air-fuel technology created similar NO_X levels.

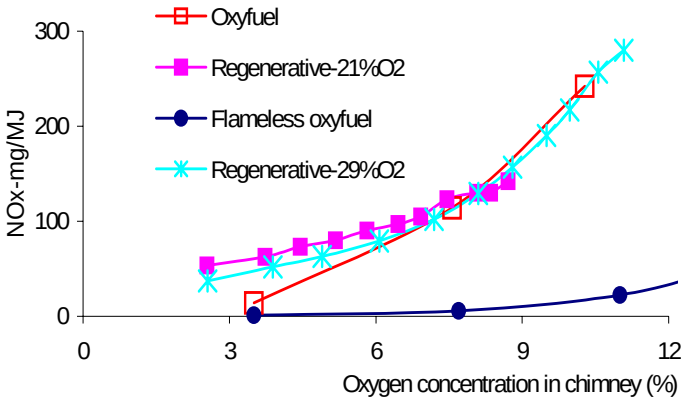

Figure 4. Emissions for conventional oxyfuel are comparable to regenerative air-fuel technology, whereas flameless oxyfuel remains almost insensitive to ingress air.[4]

Power in a small package

Oxyfuel burners have always been both powerful and compact. The new generation of flameless oxyfuel burners has maintained its compact design to facilitate exchange of already installed oxyfuel burners and for easy retrofit of air-fuel installations. Two flameless oxyfuel burner type are shown in Figure 5.

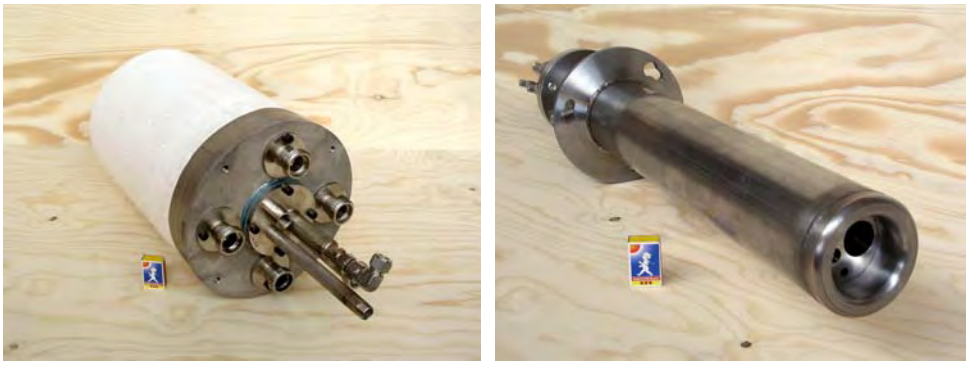

Figure 5. The photo to the left shows a 3 MW, self-cooled ceramic flameless oxyfuel burner. The photo to the right shows a compact water-cooled burner. Both are equipped with an integrated UV cell and a pilot burner.

Results in stainless steel production

Since the first flameless oxyfuel installation in 2003, this technology has proven to surpass the already and earlier recognised important benefits of conventional oxyfuel combustion; high heat flux with thermal efficiency for increased capacity, reduced specific fuel consumption, and more uniform heating.

The results from full-scale industrial installations of flameless oxyfuel in reheating and annealing furnaces during the past five years, can be summarized as follows:

- More uniform heating for improved downstream processing
- Shorter heating cycles (increased production capacity and flexibility)
- Ultra low emissions of NO_X even with ingress air

Please note that the increased production capacity can also be used as flexibility tool.

Flameless oxyfuel has also been installed for preheating of ladles and converters at a number of steel mills, including companies like Acerinox, Outokumpu and Sandvik. As described above, this technology is insensitive to ingress air with regard to NO_X formation, which is typical in vessel preheating where lids seldom close tight. More uniform heating supports shorter heating cycles and limits the need to superheat the steel melts in the electric arc furnace. Currently five steel mills use flameless vessel preheating. Ladle preheating using oxyfuel is common technology – using flameless oxyfuel technology is a milestone in preheating!

The following are examples of applying flamess oxyfuel in industrial scale operations.

Outokumpu, Degerfors, Sweden, walking beam furnace

In 2003, a walking beam furnace was rebuilt and refurbished in an AGA turnkey project with performance guarantees (Figure 6). It entailed replacing the air-fuel system (including recuperator) with flameless oxyfuel, and installation of essential control systems.[5] The resultant 40-50% increase in heating capacity provided increased loading of the rolling mill, reduction of over 25% in fuel consumption and NO_X emissions below 70 mg/MJ.

Figure 6. Outokumpu Stainless in Sweden increased their heating capacity in the existing walking beam furnace by 40-50% when implementing flameless oxyfuel (fuel: LPG). With this investment in an existing furnace plate mill could accumulate production volumes from another site.

Outokumpu, Nyby, Sweden, catenary furnace

At the Outokumpu's Nyby plant, there are two catenary furnaces, originally installed in 1955 and 1960 respectively. The catenary furnace on the first annealing-pickling line, for hot or cold rolled strips, was converted to all oxyfuel operation in 2003. Requirements for increased production combined with stricter requirements for low NO_X emissions led to this decision. The furnace, 18 m long, was equipped with flameless oxyfuel burners (Figure 7). The total power input, 16 MW, was not altered when converting from air-fuel to oxyfuel, but with oxyfuel the heat transfer efficiency increased from 46% to 76%. The replacement of the air-fuel system, combustion blowers and recuperators resulted in a 50% increase in heating capacity without any increase in the length of the furnace, a 40% reduction in specific fuel consumption, NO_X levels are below the guaranteed level of 70 mg/MJ.

Figure 7. Flameless oxyfuel burner installtion at Outokumpu, Nyby (fuel: oil).

Outokumpu, Avesta, Sweden, catenary furnace

At Outokumpu's Avesta Works, stainless sheets are hot-rolled in the Steckel mill and cold-rolled in the Z-high mill. At Avesta Works we also find the world's largest oxyfuel fired furnace, 39 MW (Figure 8).

Figure 8. Flameless oxyfuel burner installation at Outokumpu, Avesta Works (fuel: oil).

The old 24 m furnace had a 75 t/h capacity, but the requirement was to double this whilst at same time meeting strict requirements for emissions. The refurbishment included a 10 m extension, yet production capacity was increased to 150 t/h. The conversion involved the removal of air-fuel burners and recuperators and the installation of all oxyfuel. The oxyfuel technology used involved staged combustion. The conversion reduced fuel consumption by 40%, NO_X levels are below 65 mg/MJ. This furnace is an example of another route to flameless; stepwise it is now being converted from conventional oxyfuel to flameless oxyfuel.

Vessel preheating

At Acerinox, Spain, 90 tonne ladles are dried and preheated with a 2 MW flameless oxyfuel burner (Figure 7). When drying the ladles from cold status to the final temperature of 1,175°C an average thermal efficiency of 84% is reached. Preheating from about 900°C up to 1,175°C takes about 1 hour.

Figure 7. Ladle drying and preheating with flameless oxyfuel at Acerinox, Spain (fuel: natural gas).

At Outokumpu Avesta Works, 90 tonne ladles are preheated with a 1.5 MW flameless oxyfuel burner since 2004.

At Sandvik, Sweden, a 80 tonne AOD converter is preheated with a 1.4 MW flameless oxyfuel burner since 2003. The flameless oxyfuel system replaced an old 6 MW air-fuel burner system. The heating time was reduced from 13 h to 10 h, i.e. a reduction in fuel consumption of > 80% and at the same time a heating time reduction of 23%.

Summary

Flameless oxyfuel combustion has such major advantages that this process is likely to be installed in most applications. The advantages of conventional oxyfuel combustion are combined with those of flameless combustion to produce improved heating and reduced NO_X emissions. The latter advantage is normally important in the case of large, continuously operating reheat and annealing furnaces but is also relevant to other heating processes, for example the drying and preheating of ladles and AOD converters.

The development of flameless oxyfuel combustion has been brought forward in close cooperation with steel producers, i.e. the users, to meet their needs. It builds on the many proven advantages of oxyfuel over air-fuel, which have been well known for years. Since the first commercial installations in 2003, the introduction of flameless oxyfuel has taken this a step further, with even higher production rates, very low NO_X emissions and uniform heating.

References

[1] R. Eichler: “Recent developments in oxy-fuel technology for heating furnaces”, Proc. IFRF’s 25th ToTeM, Stockholm, Sweden, 2003, p.2-7

[2] “Low emissions gas fired burners”, Article in Tecno Impianti number 3, 2002, published by Editoriale Elsevier

[3] W. Blasiak, K. Narayanan, W. Yang: “Evolution of new combustion technologies for CO_2 and NO_X reduction in steel industries”, Air Pollution 2004, Greece, 2004

[4] N. Krishnamurthy, W. Blasiak, A. Lugnet: “Development of high temperature air- and oxyfuel combustion technologies for minimized CO_2 and NO_x emission in industrial heating,” Joint International Conference on Sustainable Energy and Environment, Dec.1-3, 2004, Hua Hin, Thailand, vol. II, p. 552-557

[5] S. Ljungars, M. Gartz, J. von Schéele: “Boosting heating capacity using new technology”, Nordic Steel&Mining Review, Sweden, 2004, p.49

HYDROGEN REDUCTION OF STAINLESS STEEL SURFACE OXIDES

S. Ahonen[1], C. Laumen[1], S. Wiberg[2]

[1]Linde AG, Germany, [2]AGA Gas AB, Sweden

Abstract

The formation of oxide scales in hot forming operations, such as hot rolling, creates material losses and extra operations to remove the scales. Various acids are used in the removal process and due to environmental reasons their use is becoming less attractive. One ecological way to replace acids in the near future can be high temperature reduction in hydrogen.

In these trials the focus was on the hydrogen reduction of annealing oxides and the study was carried out in a laboratory scale furnace. Five different steel grades from low alloyed carbon steel to high alloyed duplex stainless steels were studied.

Results from the trials were encouraging as all the samples had bright surfaces after the treatment. Both iron oxides and iron-chromium oxides were reduced. The reduction time was dependent on the total amount of the oxide, oxide composition and the reduction temperature. In some samples the surface chromium content was increased due to oxide reduction and back diffusion. On corrosion point of view the increased surface chromium content should be a positive phenomenon.

Hydrogen reduction works out well as a pre-treatment process because it dramatically reduces the total time used for pre-treatment and mixed acid pickling when compared with salt-bath pre-treatment. It remains to develop a technical and cost effective industrial process solution.

Introduction

Using hydrogen reduction instead of acid pickling for surface oxide reduction can become an attractive alternative. It was studied already 15 years ago [1] and the results were very promising. Reduction of Fe_2O_3, Cr_2O_3 and mixed spinel oxides were resulting in these trials. In a recent study chromium oxide layer was removed from austenitic stainless steel wires by hydrogen reduction [2].

In order to simulate the actual industrial processes, both batch and continuous ones, two different kinds of trials were done in this project. In the “batch type” trials the samples were heated up to the reduction temperature and then held in that temperature. In the “continuous type” trials the samples were put into a furnace which was already heated up to the reduction temperature.

Experimental

Material

All the materials studied in this project were in production annealed condition. Product dimensions are shown in Table 1 and the nominal compositions are presented in the Table 2. The wires were all hot rolled while the strip material was cold rolled.

Table 1. Materials used in the trials

Sample	Steel grade	Sample type	Company	Diameter/thickness
TA	20AP	Wire	Sandvik MT	6,0 mm
TB	11R51 (302)	Wire	Sandvik MT	5,5 mm
TC	304L	Wire	FSAB, Sandvik MT	5,5 mm
TD	Nikrothal 40	Wire	Kanthal	5,5 mm
TE	2205	Wire	FSAB	6,0 mm
BE	2205	Strip	Outokumpu Stainless	0,95 mm

Table 2. The alloying of the researched materials

Steel grade	C	Si	Mn	P_{max}	S_{max}	Cr	Ni	Mo	N	Pb
20AP	1,0	0,2	0,4	0,05	0,05					0,2
11R51	0,08	1,5	1,8	0,025	0,015	17	7,5	0,7		
304L	0,02					18,1	8,3			
Nikrothal 40	<0,10	1,6-2,5	<1,0			18-21	34-37			
2205 wire	<0,03	<1,0	<2,0	0,030	0,015	22	5,5	3,2	0,18	
2205 strip	0,019	0,41	1,52	0,022	0,02	22,51	5,76	3,25	0,168	

Annealing conditions

Hydrogen reduction tests were carried out either by heating up the samples 0.5ºC/s to 1200ºC or heating in a hot furnace (1100ºC). The diameter of the quartz tube furnace was 42 mm and the reduction was studied with two different hydrogen flow velocities: 4 and 8 l/min.

Exhaust gas composition was measured with a PAS analyser (Photo Acoustic Spectrometer). Detection minimum for water is 0.1 ppm and for CO, CO_2 and CH_4 around few ppm. The PAS graphs gave the general picture about the reduction of different oxides.

Analysing methods

In order to get a clear picture of the composition, thickness and morphology of the oxides, a combination of surface analysis techniques were used for analysing the oxides before and after the hydrogen reduction.

Oxides and surfaces were studied with a scanning electron microscope (SEM). A more thorough analysis was done with a GDOES (Glow Discharge Optical Emission Spectroscopy), which gave a general average from the whole analysis area, this case 2 mm of diameter. In addition, powder X-ray diffraction with for the scraped oxide from the annealed samples was performed.

Results

The resulting graphs from the measurements showed two types of peaks. Peaks at low temperature, starting at 350-400°C, are representing the reduction of iron oxide. Peaks at higher temperature, starting at 800°C, are resulting from the reduction of chromium rich spinel M_3O_4 and chromium oxide Cr_2O_3. (M equals Cr, Fe and Mn in different proportions).

20AP

The oxide of 20AP consists mainly of iron oxides and the first iron oxide reduction peaks were seen at 250°C. Propable oxide thickness by GDOES was estimated to be 3.8 µm. The normal annealing temperature for 20AP is 800°C and the oxides were reduced after 2-3 minutes. With the higher temperature, 1000°C, the reduction time was shorter (1-2 min). A comparison between the two annealing temperatures of 20AP showed that the higher temperature results in a cleaner metal surface and that the holding time can be lowered significantly.

Photos of the samples after the hydrogen reduction in Picture 1 show a bright and relatively smooth surface. SEM research showed silicon enrichment on the reduced surface. Large flakes with silicon enrichment and iron reduction were loosely attached to the surface and they had partly come loose or folded. GDOES analysis shows that silicon has diffused and enriched the outer surface (ca. 0.05 µm) and created underneath a silicon-poor layer. Silicon content restored back to normal at ca. 0.5 µm.

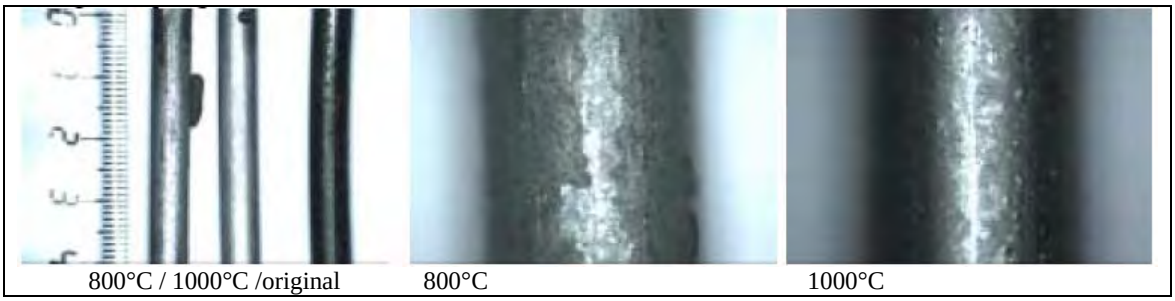

Figure 1. Photos of the 20AP samples from batch type hydrogen reduction

11R51

11R51 is an austenitic steel, which forms in hot rolled condition mainly iron-rich spinel oxides with Fe_2O_3 and Cr_2O_3. Oxide thickness according to GDOES was 1.5-4 µm. PAS graphs showed two very clear peaks for Fe-rich and Cr-rich oxides. After the heat treatment the wires were bright as shown in Picture 2 and according to SEM there were both chromium and silicon enrichment at the surface. From the oxide free surface a chromium content of 22-24% was measured, which is significantly higher than to nominal Cr-content (17%). Like with the 20AP there was a thin partly scaled off surface.

Figure 2. Photos of the 11R51 samples from batch type hydrogen reduction

Nikrothal 40

Oxides on the hot rolled Nikrothal 40 wire were quite similar to the ones on 11R51. Fe was the main component of the oxide and there were also small Cr enrichment. XRD gave a clear identification of spinel oxide on Nikrothal with certain element of Cr_2O_3. Oxide thickness in the material before the hydrogen reduction was measured to be 4.7 µm.

The sample was bright after the hydrogen annealing as can be seen in Picture 3. Both SEM-EDS and GDOES showed clear silicon enrichment on the reduced surface. Edges and flakes on the surface are containing higher amounts of silicon. To understand the hydrogen reduction it is important to analyse how silicon oxide is divided in the material of delivered state. Silicon oxide particles can be formed under the oxides or in the grain boundaries and the form is expected to have a major importance for results in hydrogen reduction.

Figure 3. Photos of the Nikrothal 40 samples from continuous type hydrogen reduction

2205 wire

Hot rolled 2205 wire had only a small amount of oxide and it was seen in the X-ray diffraction that the peak tops are from the metal and not from oxides. Nevertheless there were very small peaks which are corresponding to several oxide types.

PAS graph gave a good correspondence since there was only a small water peak from the reduction of Fe-containing oxides during the heating phase. After the annealing the surface was bright as Picture 4 shows. There was also enrichment of both chromium and silicon. In the trials the austenite has transformed into ferrite and essential grain growth has also occurred because of the high annealing temperature 1200°C. Normal temperature for a duplex structure would be 1070°C). It is also important to control the cooling rate from the annealing temperature when handling duplex steels.

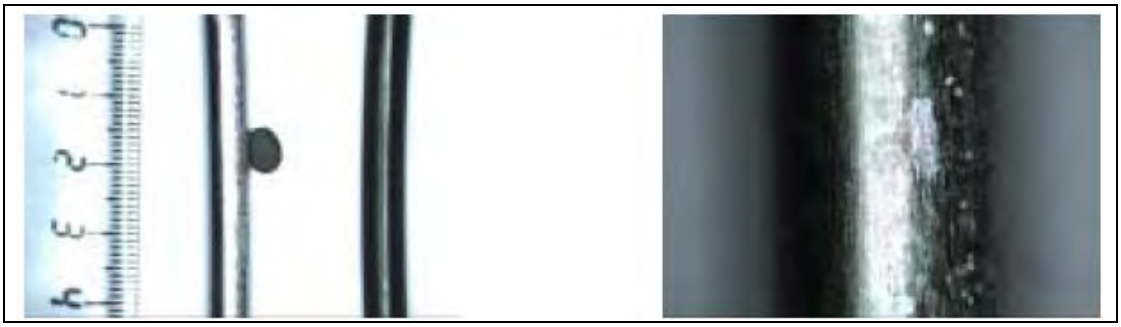

Figure 4. Photos of the 2205 wire samples from continuous type hydrogen reduction

2205 strip

The 2205 strip material has been studied in previous projects [3] and the material differs from the other samples since it is bright annealed. The total oxide layer thickness was ca. 0.5 µm and the underlying duplex structure did not have an effect on the oxide. In the boundaries between the metal and the oxide there were presence of SiO_2 and/or Fe_2SiO_4, which are formed when the oxygen partial pressure is too low for chromium oxide formation.

In the annealing trials only one or two small water peaks from oxide reduction were seen with high temperatures (over 900°C). This is very well correspondent with the fact that only chromium containing oxides were found on the samples. Sample surfaces were bright after the annealing, Picture 5. The surface showed only a slight enrichment of silicon with the depth of <0.5 µm. As before with the 2205 wire, also the strip material had experienced grain growth at the annealing temperature 1200°C.

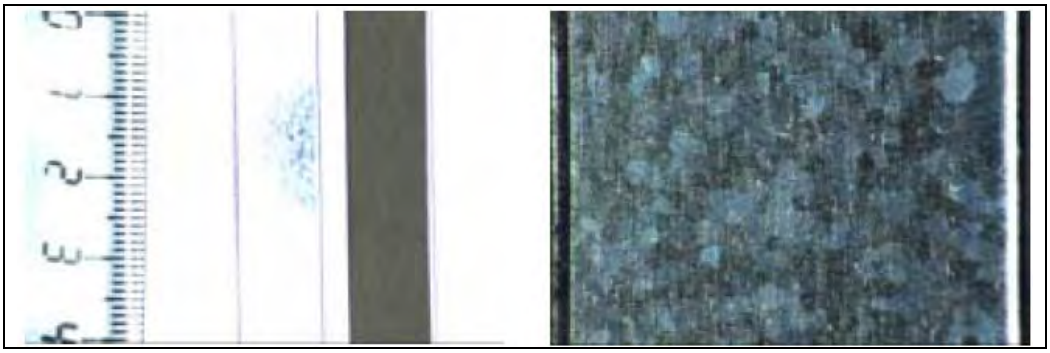

Figure 5. Photos of the 2205 strip samples before and after the hydrogen reduction

304L

304L wire was taken from a previous investigation [3]. Oxide thickness varied between 15 and 25 µm and included both M_2O_3 and spinel oxides (M_3O_4) according to XRD. The outer M_2O_3 component had 70% of iron and traces of other alloying elements while the underlying spinel oxide contained both iron and chromium.GDOES analysis of these studies verified this picture and the oxide thickness was evaluated to be 11 µm.

PAS graphs show that the oxides on 304L are mainly reduced in 10 minutes. Shorter annealing times (8 min, 4 min and 3 min) were used to study the influence of partial oxide reduction. After 8 minutes in the furnace the material had a bright metallic surface, Picture 6. Even shorter reducing times left still a visible surface oxide.

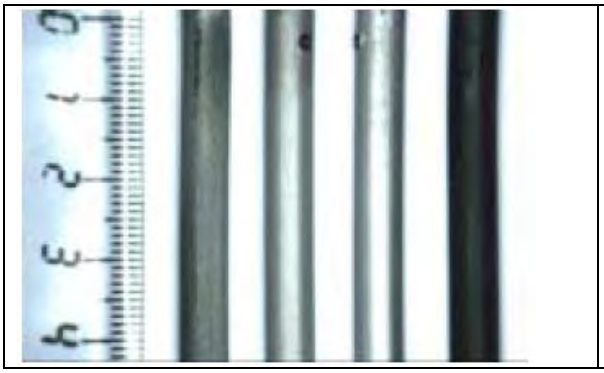

304L in 1100°C furnace.
Samples from left to right:

1. 3 minutes
2. 4 minutes
3. 8 minutes
4. original oxidised wire

Figure 6. Photos of 304L after the hydrogen reduction with different reduction times at 1100°C

SEM-EDS investigation was done for two 304L samples. The samples which had been annealed only 3 minutes showed chromium oxides due to longer reduction time of Cr-oxides. The samples with 8 minutes annealing included less oxides and had only SiO_2 and/or Fe_2SiO_4 at the surface. Chromium enrichment can be seen also on the almost oxide-free surface. An interesting question is whether this higher chromium content can improve the corrosion resistance properties.

To study how gas flow effects on the oxide reduction a trial was done with together bound wires of 304L. Seven relatively straight rolled wires with the length of 150 mm were tied together to a tight bundle and then reduced with batch type process for 20 minutes.

When wire bundle was opened the wire sectors which had been contacting each other were clearly visible, Picture 7. The reduction of oxides is very dependent on the hydrogen gas access to the surface. In this trial however no directed hydrogen gas convection was used inside the wire bundle, which should improve the results.

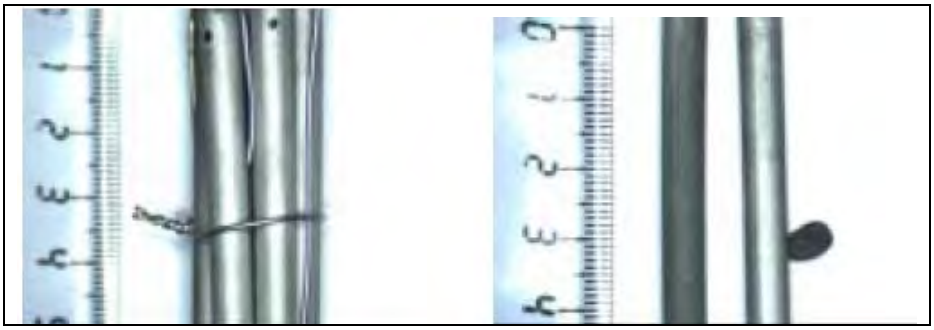

Figure 7. Photos of the 304L bundle and the wires after the hydrogen reduction

Comparison of the oxide thicknesses

Oxide thickness was evaluated from the GDOES graphs. The results are shown in Table 3. Profiles showed lower oxide thickness after the hydrogen reduction than in delivered state.

Table 3. GDOES evaluation of oxide thicknesses on samples in delivered state

Material	Oxide thickness in delivered state (µm)		Oxide thickness after H_2 reduction (µm)	
	At 5% oxygen	50% of oxygen maximum	At 5% oxygen	50% of oxygen maximum
304L	11,18	1,46	0,15	0,02
2205 strip	0,47	0,28		0,007
20AP	3,81	0,31		0,004
Nikrothal 40	4,68	0,86		0,03
11R51	3,82	1,52		0,006

Conclusions

Results show that during hydrogen annealing the oxides containing high amounts of iron or chromium are clearly reduced. This process is relatively fast and it has a great potential to compete with the existing pre-treatment or pickling processes. It is easy to reduce just iron oxides since they do not require low dew point or high temperature. On the contrary both low dew point and high temperature are needed to for chromium oxide reduction. For example Cr_2O_3 can be expected to reduce around 800°C with 1 ppm H_2O and around 1000°C with 100 ppm H_2O. Reduction of SiO_2 requires even lower dew point at high temperatures (1000°C). It is not clear if the presence of SiO_2 is just a disadvantage, since for example in wire drawing it might be beneficial.

Highly promising application for hydrogen annealing is to replace the salt bath treatment on wire, which is used as a pre-treatment before mixed acid pickling. The test with 304L showed that the total treatment time for hydrogen reduction + mixed acid pickling was shorter than making the treatment in reducing and oxidising salt baths.

The following work needs to concentrate on bringing the test scale closer to the real process scale and optimising the process parameters and product properties for different steel grades.

References

[1] P. Miholich: “Hydrogen annealing of stainless steel as alternative to pickling”, AGA report REPM 93407, 1992
[2] A. Salwen: Kinetic studies of hydrogen reduction on hot rolled and batch annealed stainless steel wire at KIMAB, 2006
[3] R. Pettersson et al.: Oxidation and pickling of stainless steels in a new annealing process IM-2003-517, STEM43022.

STUDY ON THE LAYERS IN THE FILM ORIGINATING FROM THE CASTING POWDER BETWEEN STEEL SHELL AND MOULD AND ASSOCIATED PHENOMENA IN CONTINUOUS CASTING OF STAINLESS STEEL

P.O. Hooli

Tornio Research Centre, Outokumpu Tornio Works, Finland

Abstract

Studies were conducted in order to examine the properties of films between the mould and steel shell during the continuous casting of stainless steel. Film sampling was carried out in the tail-out phase at the end of the cast. The films were subjected to chemical analyses and respective compounds and phases were determined. Local heat fluxes were measured with thermocouples and the resulting data was subjected to analyses.

Several massive samples were collected, a number of which were several millimetres in thickness and covered virtually the entire width of the mould, descending 40cm below the meniscus.

The most typical feature in the sampled films was the layer dominated by a cuspidine phase. The most unexpected feature was the formation of a separate NaF layer, and the formation of elemental Na against the mould wall. The study found that the films could have residence times of as much as several hours on the mould wall, and complex structures containing several sub layers, voids and pores can develop. Evidence of fracturing was found in the sampled films.

Introduction

The main purpose of the casting powder is to create lubricating layer between the steel shell and the mould by infiltrating in to the gap between those. Part of liquid slag is re-solidifying on the mould wall forming a solid film and thus lubrication in a fact occurs between the steel shell and this film. The formed solid film has an influence on lubrication, heat removal and surface quality. This study was made in order to find the role of the film on those items.

Experimental

The experimental part of the work was performed at Outokumpu Tornio Works in casting machine No. 1. Samples were taken from this film with the special sampling method developed. Steel grades used were AISI 304, 316, 321 and 316Ti.

Compositions of the used casting powders based on information by suppliers were as follows (ranges of main compounds): 30-32 mass% SiO_2, 32-37 mass% CaO, 5.3-6.8 mass% Al_2O_3, 7-9.3 mass% Na_2O and 6.3-7.5 mass% F

One of the moulds was also equipped with thermocouples in the lower part of the copper faces. Temperatures recorded by thermocouples were used to observe local heat fluxes in different areas of the mould.

Flux films

Solidifying of steel is started in the mould and for this purpose heat must be removed from liquid steel to cooling water. Heat flux from liquid steel must pass except steel shell and mould wall, also slag layers and possible air gap as shown in Figure 1, where some of associated phenomena in the mould are also shown.

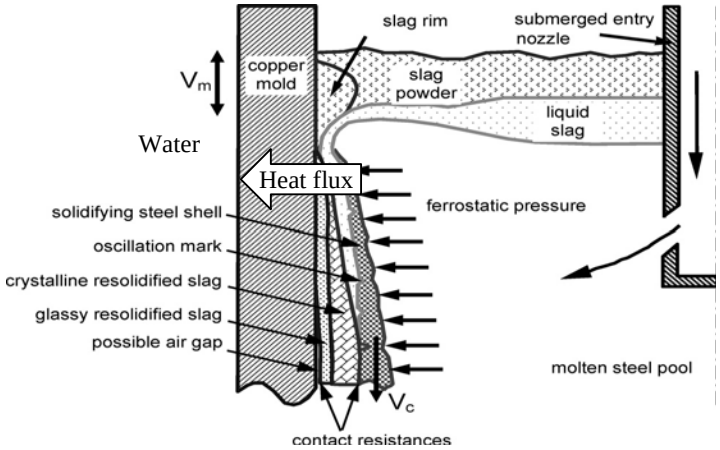

Figure 1. Schematic representation of the various slag layers formed in the mould, steel flows and associated parameters.[1]

A schematic illustration of the slag film based on the taken samples is shown in Figure 2.

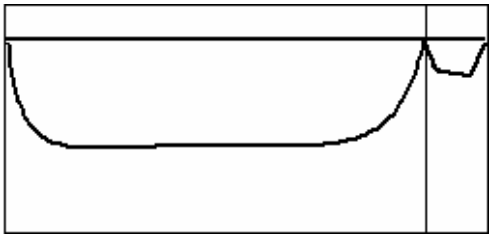

Figure 2. Typical shapes of the flux layers shown schematically on the wide and narrow faces of the mould.

On the narrow faces and near the corners of the mould the slag film was shorter and also thinner. Thickness of the film was up to 4 mm including layer formed during tail-out, which was most often the major part of the sample (see Figure3).

The photo collage shown in Figure 3 presents a survey of the properties of the structures, which were microscopically visible. Two series of photographs are shown. In the left series, photographs came from a cast with a total casting time of approximately 2 hours, which involved two heats. The right series represents a cast of approximately 5 hours, involving five heats. The photographs are presented in order of their distance from the meniscus.

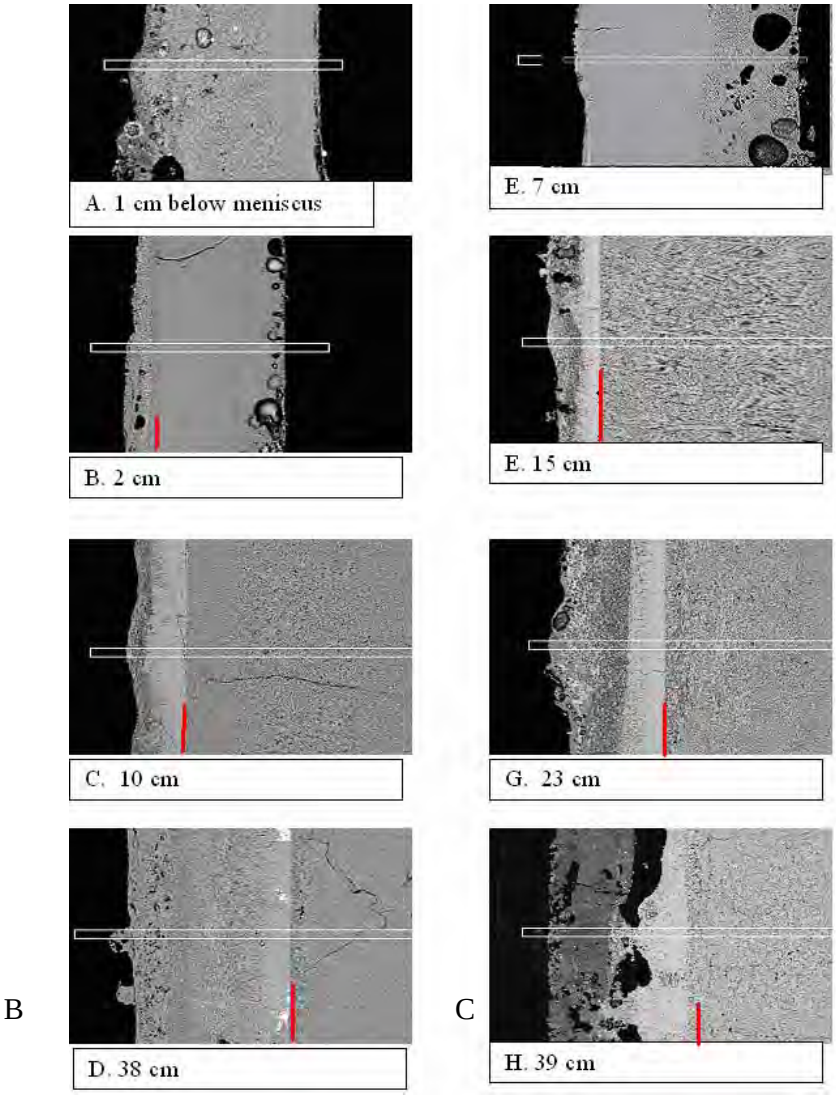

Figure 3. Two series of the layer cuts of films from two casts with different distances from the meniscus. The series on the left is from a 2 hour cast; that on the right is from a 5 hour cast. Layers right from the short lines are formed during tail-out.[2]

Layers in the sampled films can be separated first to two main sub layers: one formed during the tail-out (layer 0 in Figure 4), and second, prime layer, formed during the casting. The layer formed during casting can contain several sub layers, as shown in Figure 4 (1-4). It may be assumed that the layer 1 was the liquid, lubricating layer during casting. In the layer 2 cuspidine phase is dominating. In the layer 3 there are cuspidine and nepheline phases and pores. The layer 4 contains NaF phase and numerous voids.

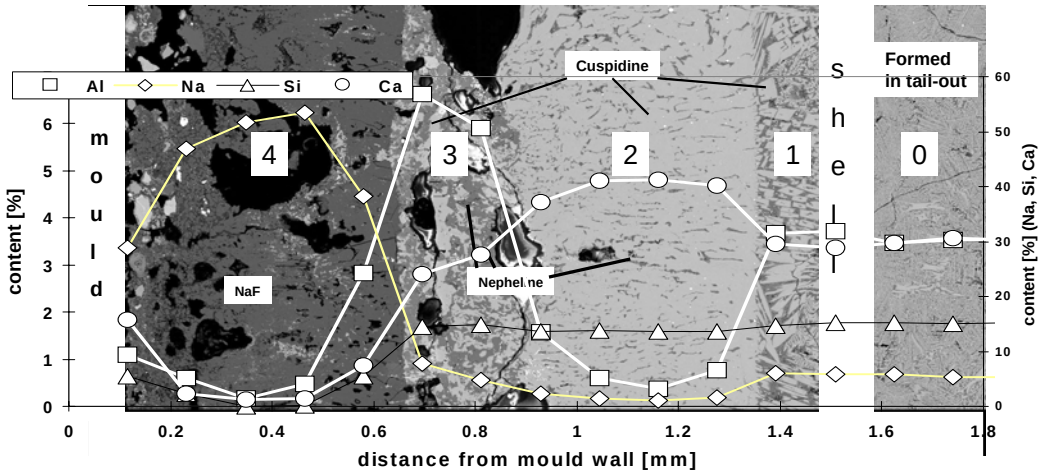

Figure 4. The average concentrations of some elements in different layers in the film shown in Figure 3H.

Heat transfer

Heat transfer from liquid steel to the cooling water is one of the most essential tasks in the mould. Temperatures of thermocouples (i.e. heat flux) could decrease in some of the casts on certain locations substantially, as shown in Figure 5. Reasons for those drops in the heat flux were increased thickness and chances in the structure of the flux film.

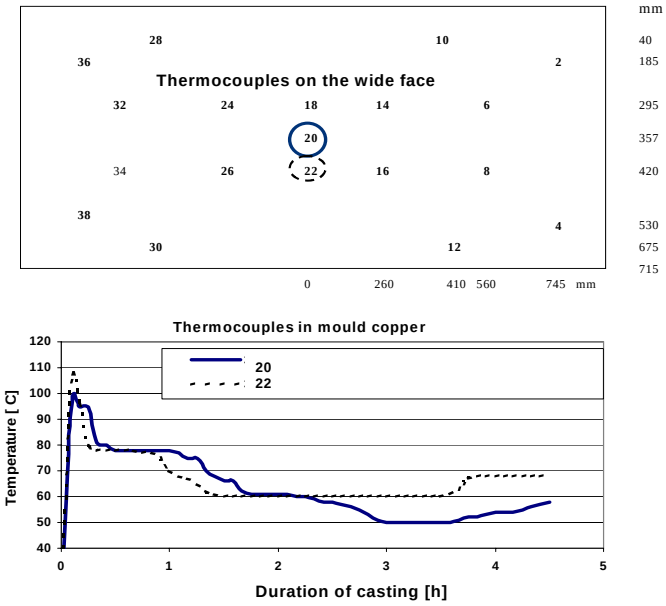

Figure 5. Locations of thermocouples and behaviour of temperatures at two locations during casting of 5 hours.

Thus the flux film between the steel shell and the mould has an important role concerning the heat flux from the steel shell to the mould. Using a spreadsheet, temperature gradients and temperatures in different points in the flux film structure were calculated for some of the observed layers. In Figure 6 results shown for the films shown in Figures 3 D and H (cases B and C in Figure 6). The third case represents conditions at the beginning of casting (A). Values of the heat fluxes were adjusted based on the temperature of the thermocouple situating in the same location as the observed films (about 38 cm below meniscus).

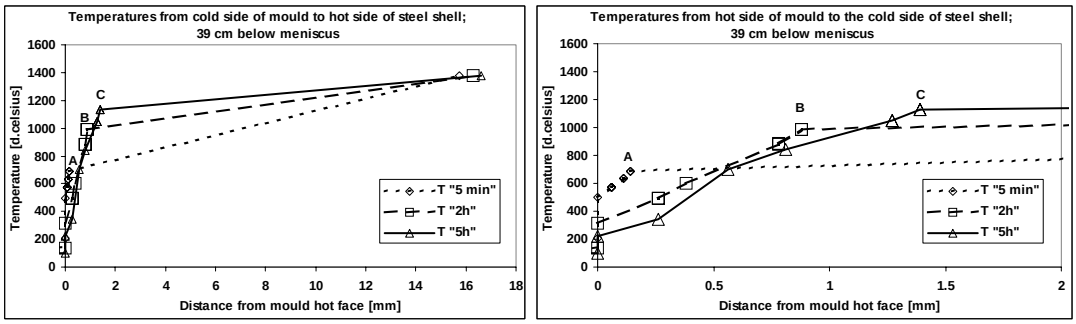

Figure 6. Temperature gradients of three cases from hot surface of mould a) to the inner side of steel shell and b) to the outer side of steel shell b). (so b) is part of a)).

From these calculations, it is possible to state that the layers observed can serve as an explanation of these very low heat fluxes (i.e. low temperatures recorded as shown in Figure 5).[3]

Fracturing of the film

When the flux film is increasing in thickness, it can come into the state where it starts to fracture. In Figure 7 there are a solid, unbroken film, and two fractured films shown. In Figure 7b the whitish cuspidine layer has broken into several short pieces and in the case c only some spots are left in the later formed film (formation of the structure of the film shown in Figure 7a takes time). Fractures in the film can lead to problems in the lubrication and finally sticking of the shell to the mould.

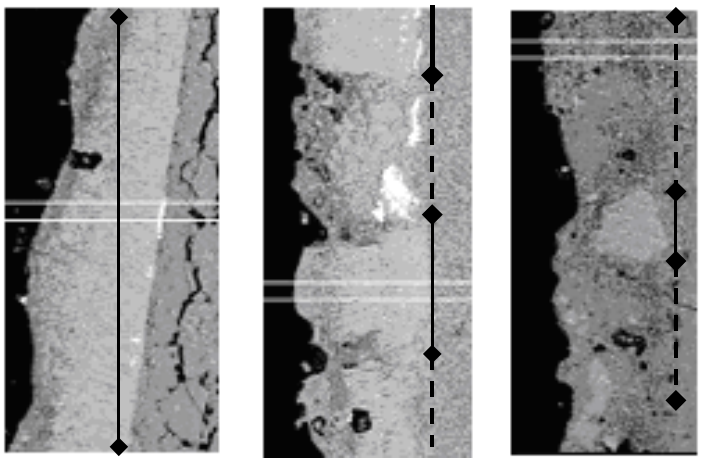

Figure 7. Examples of flux film structures showing unbroken and fractured films (a,b and c).

Surface quality of slabs

The flux film can have also influence on surface defects, as shown in Figure 8. The number of the slag defects are on a higher level with increasing casting time probably because the increased flux film thickness has caused changes in the lubricating layer. It should be noted that the casting powder used in the case of Figure 8 is not anymore in use.

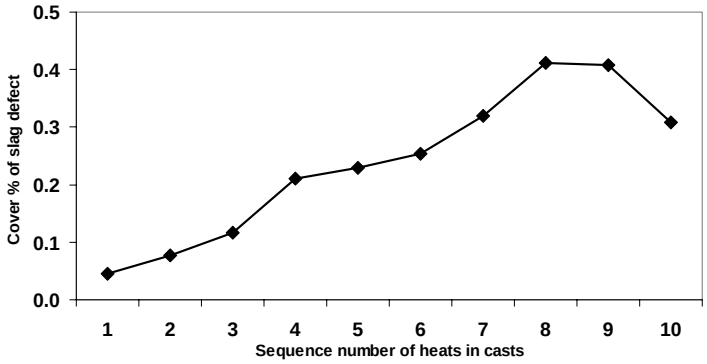

Figure 8. So-called cover % (i.e. % of the total length of the strip covered with the slag defect) vs. duration of casting. (In this case, one heat corresponds to approximately one hour of time, AISI 304).[3]

Conclusions

Some typical features were observed in the films: phases cuspidine, nepheline and NaF, and additionally pores and voids.
Formation of the solid flux film in the gap between the shell and the mould has influence on the heat removal and stability of lubrication, and quality of slab surface.
This method used in this study to have samples and analysing them can be used for evaluating the functioning of different casting powders.

References

[1] Y. Meng, B.G. Thomas: 'Simulation of microstructure and behavior of interfacial mold slag layers in continuous casting of steel', ISIJ International, Vol. 46, No. 5, 2006, pp. 660-669.
[2] P. Hooli: 'Study of the Mould Flux Film between Mould and Steel Shell', Sixth International Conference Molten Slags, Fluxes and Salts, Stockholm-Helsinki, 2000.
[3] P. Hooli: "Study On The Layers In The Film Originating From The Casting Powder Between Steel Shell And Mould And Associated Phenomena In Continuous Casting Of Stainless Steel.", Doctoral Thesis, Helsinki University of Technology, Department of Materials and Engineering, Laboratory of Metallurgy, 2007, p.79.

METALLURGICAL SLIVERS IN T304 AUSTENITIC STAINLESS STEELS

C.I. Garcia[1], M.J. Hua[1], A.J. DeArdo[1,2]

[1]University of Pittsburgh, USA, [2]University of Oulu, Finland

Abstract

Metallurgical slivers have been a persistent problem in the production of high-quality austenitic stainless steel sheet in both hot rolled or cold rolled gauges. Recent studies on commercial slabs of T304 and T316 austenitic stainless steels have shown that there are several metallurgical and process variables that contribute to the formation of these surface defects. These include slab composition, surface grinding practice, reheating furnace atmosphere, drop-out temperature, and hot rolling practice. The overall particular practice considered here is that which converts cold charged 200-250 mm thick slabs of T304 and T316 and chemical variants to 2 mm cold rolled and annealed sheet product. The results of this study show that there are two metallurgical conditions that are necessary for high susceptibility for sliver formation: (i) suppression of recrystallization of the as-cast and reheated columnar grain structure during rough rolling and the subsequent large grain size present upon entering the first finishing rolling pass and (ii) weakened delta-delta ferrite (δ-ferrite) dendritic grain boundaries. This susceptibility is further accentuated by high sulfur contents and poorly conditioned slab surfaces and geometries. When these conditions are present, a high frequency of sliver formation can be expected. This paper will discuss each of these factors, including their description, origins and possible ameliorative actions or procedures.

Introduction

Slivers are surface defects that can be caused by several sources. Their occurrence represents significant economic loss each year to the stainless steel producers. In the research program described below, hundreds of commercially produced slabs and coils were visually inspected for metallurgical slivers at different stages of processing. These were chosen both randomly and as part of a long-term, disciplined production experiment. During visual inspection of steels showing metallurgical slivers, in the of slab, transfer bar, hot band or cold rolled conditions, metallurgical slivers appear as short, thin, dark lines on the otherwise bright stainless steel surface. A schematic illustration of a typical sliver defect is shown in Figure 1.

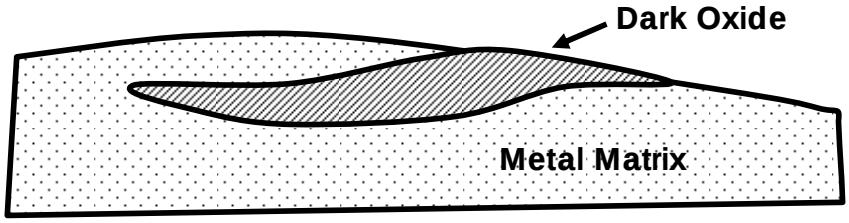

Figure 1. Schematic of typical cross-section of sliver defect.

The As-Cast Solidification Structure of T304

According to published ternary phase diagrams, steels such as T304 (18%Cr-8/10%Ni) are located just outside the δ-ferrite + γ two-phase field, in the single-phase γ field, Figure 2. [1]

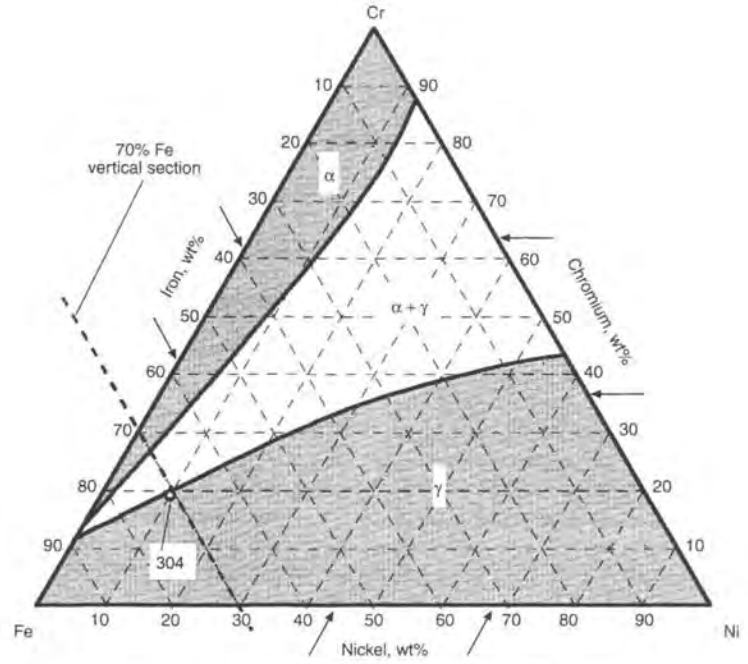

Figure 2. Isothermal section of Fe-Cr-Ni phase diagram at 1100°C (2010°F). [1]

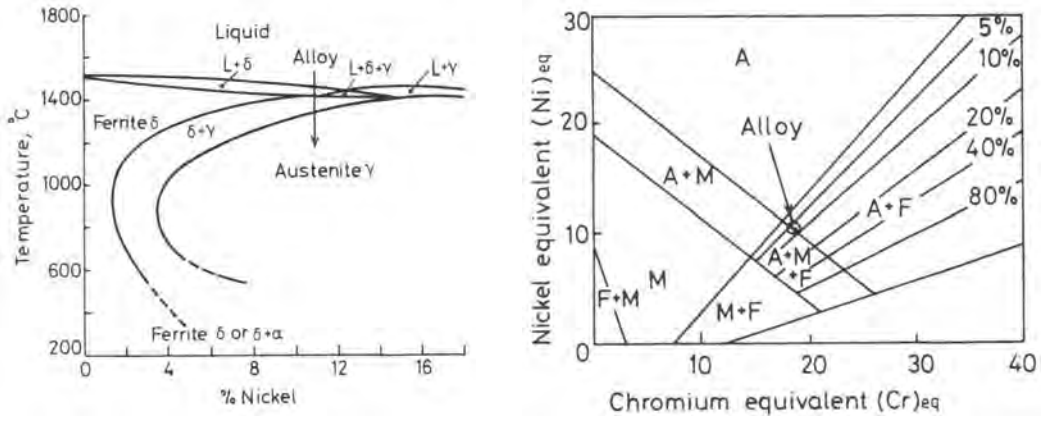

Figure 3. (a) 18%Cr section of the Fe-Cr-Ni system. b) Schaeffler diagram indicating the alloy concerned.
(Ni)eq = %Ni + 30 x %C + 0.5 x %Mn. (Cr)eq = %Cr + 1.5 x %Si + 0.5 x %Nb.
A, austenite; F, Ferrite; M, martensite. [2]

The evolution of microstructure and the resulting phase balance present at any given temperature can be approximately predicted using the pseudo-binary equilibrium phase diagram and Scheffler Diagram, as shown in Figures 3a and 3b, respectively. [2]

For T304, the 18%Cr-8/10%Ni composition would follow the following sequence of phase changes during solidification and subsequent cooling:

L > L + δ-ferrite > δ-ferrite > δ-ferrite + γ > γ (Reaction Path I)

For typical carbon (600 ppm), nitrogen (600 ppm) and manganese (1%) contents, the exact phase diagram would be set and the δ-ferrite content at any given temperature established.
T304 or T316 steel solidifies during continuous casting as δ-ferrite dendrites of large size, approximately 10 mm in diameter and 80mm in length. These dendrites partially transform to γ during cooling resulting in columnar grains of γ surrounding islands of retained δ-ferrite. This transformation proceeds by γ nucleating at the δ-ferrite grain boundaries and then growing both along the boundaries and into the δ-ferrite grains, eventually partially or completely consuming them, depending on circumstances. The extent of this transformation depends on the temperature, time and location on the ternary phase diagram. These transformations are shown in schematic fashion in Figure 4.

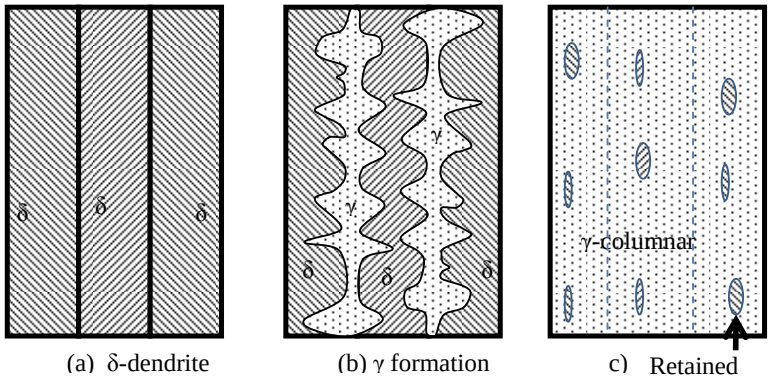

Figure 4. Schematic representation of microstructural changes associated with (a) solidification, (b) subsequent early cooling and transformation and (c) after reheating of an as-cast slab.

In conventional steel processing, the temperatures for reheating the cold charged slabs and the rolling in the roughing train will be in the upper two-phase region of Figure 4a. Subsequent hot rolling in the finishing train will take place mainly in the single-phase γ region as the stock temperature falls and rolling proceeds. The boundary between the δ-ferrite + γ and γ phase fields is near 1100°C.

This retained δ-ferrite is normally viewed in WQ specimens and is observed to be embedded in the columnar γ grains when observed at RT, as is depicted schematically in Figure 4. The δ-ferrite crystals are located at or near the center of the original δ-ferrite dendrites, on both primary and secondary arms of the original δ-ferrite dendrites after WQ following solidification and cooling to the slab torch-cutting temperature. This partially transformed structure is shown in Figure 5a, while the δ-ferrite crystals are presented in Figure 5b.

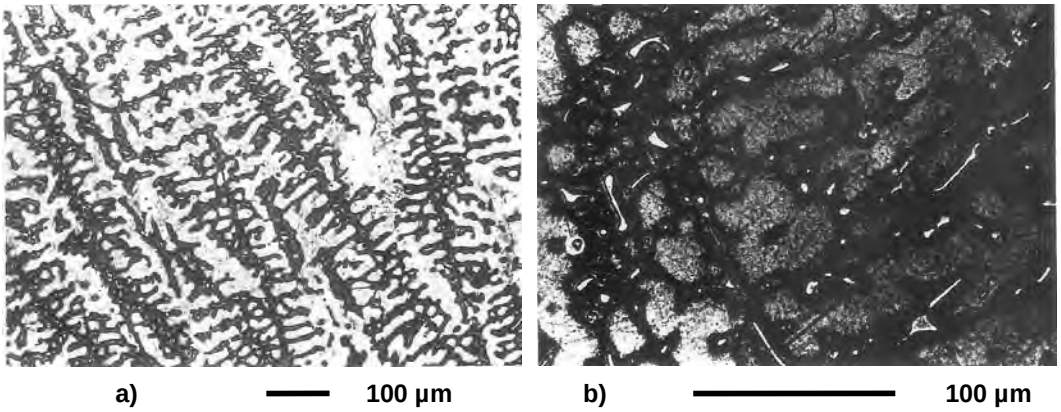

Figure 5. Optical metallographic microstructure of the as-cast condition. a) Columnar γ grains with retained δ-ferrite (oxalic acid etch) and b) the δ-ferrite from Figure 4a. Volume fraction δ-ferrite is ~ 1.9%.

Experimental Procedure

In this study, the assumption was made that slivers were the result of poor or inadequate hot ductility. Hot ductility tests were conducted using notched, flat specimens removed from slab surfaces. These specimens were tested in bending, where the hot ductility was measured as the local strain to crack initiation. The tests were run at 950°C which is approximately where the cracks were first identified in commercial practice. The thermomechanical history used prior to the hot ductility testing is based on hot strip mill practice and is shown in Figure 6. [3]

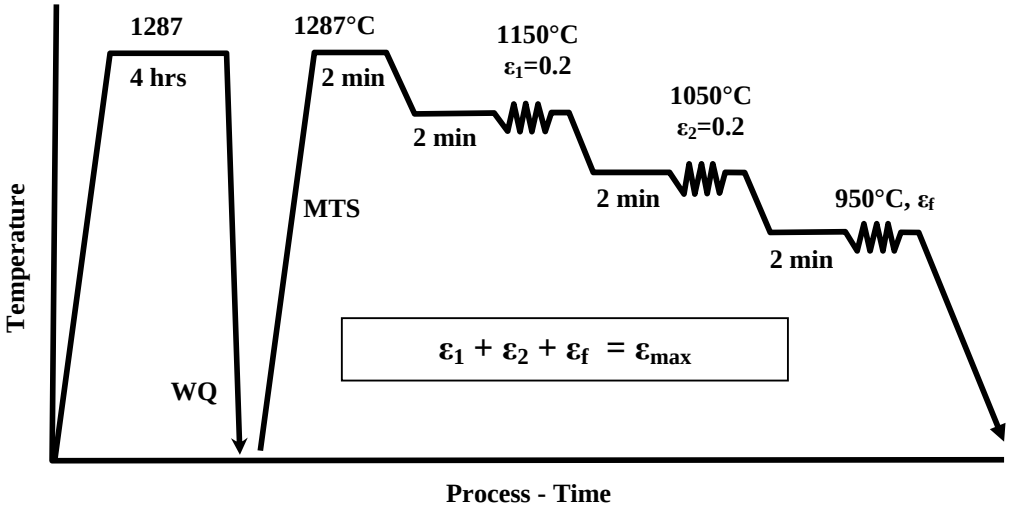

Figure 6. TMP history of specimens for hot ductility test. Hot ductility tests were run at ε_f. [3]

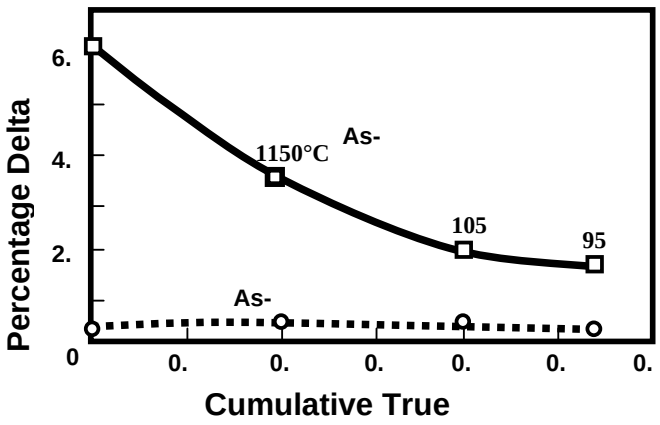

Figure 7. Effect of pre-conditioning on δ ferrite observed at various temperatures for T304 steel. Initial condition either as-cast or as-reheated prior to full hot ductility simulation.

The behavior of the retained δ-ferrite during the TMP processing prior to the hot ductility test is shown in Figure 7. Two initial conditions were studied. The first was industrially cast, reheated and cooled prior final reheating and hot ductility testing. This condition, labeled As-Reheated in Figure 10, showed very little retained δ-ferrite when cooled to 950°C. The second, labeled As-Cast in Figure 7, was water quenched to room temperature from the near-as-cast condition, prior to final reheating and ductility testing. This condition showed relatively large amounts of retained δ-ferrite at all temperatures used in the TMP pre-treatment and prior to hot ductility testing.

Because most of the deformation is occurring in the single-phase γ field, the trend expected would be for the δ-ferrite to undergo transformation to γ and the accompanying deformation would accelerate the δ-ferrite – to- γ transformation. This is what was observed, Figure 7.

Results and Discussion

The interesting and obvious relation between hot ductility and retained δ-ferrite is one area for discussion. One of the underappreciated but important roles of hot rolling, especially for the hot roughing mills, is to eliminate the dendritic or columnar grain structure before the steel enters the finish rolling train, where the stresses across the former dendritic δ-ferrite or columnar γ/γ boundaries become so high that the boundaries can be fractured. The role of these boundaries in hot ductility is shown in Figure 8, which shows the secondary cracks in hot ductility test specimens following the dendritic δ-ferrite or columnar γ/γ boundaries in unrecrystallized specimens.

It is this fracture event that is believed to be largely responsible for metallurgical slivers. Fortunately, the columnar/dendritic structure can be eliminated through static recrystallization which occurs between rolling passes, especially in the roughing train, i.e., before the steel enters the finish rolling train. When the columnar γ (or prior δ-ferrite dendritic) grain structure is obliterated through recrystallization, no easy crack paths exist for growth of nucleated cracks. The importance of recrystallization on hot ductility is shown in Figure 9.

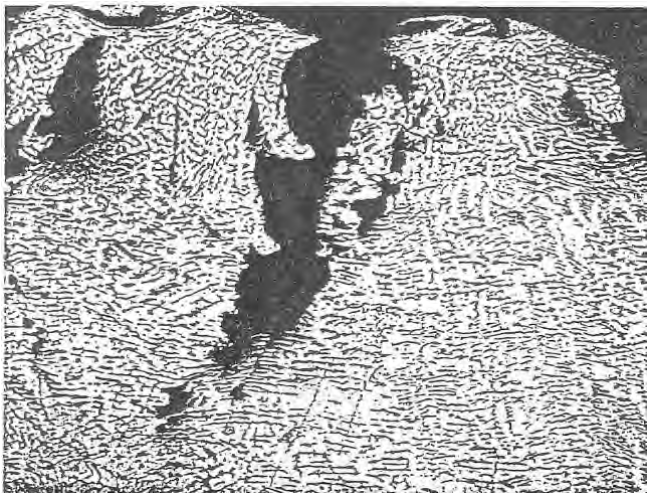

Figure 8. Optical micrograph showing cracks. Specimen taken from slab #3, Top Edge A.
Reheat at 1234°C, $\varepsilon_1 = \varepsilon_2 = 0.2$ at 1150 and 1050°C, ε_f at 950°C.

Figure 9 shows the strong effect of prior recrystallization from earlier TMP on the hot ductility at 950°C. Clearly, the higher the extent of recrystallization, the higher the hot ductility and the lower the susceptibility to sliver formation.

Finally, there is the very well-known relationship between hot ductility and grain size, even in specimens that had undergone recrystallization prior to hot ductility testing, Figure 10. This type of relationship has been observed in many studies of hot ductility across a broad spectrum of steels [4-13].

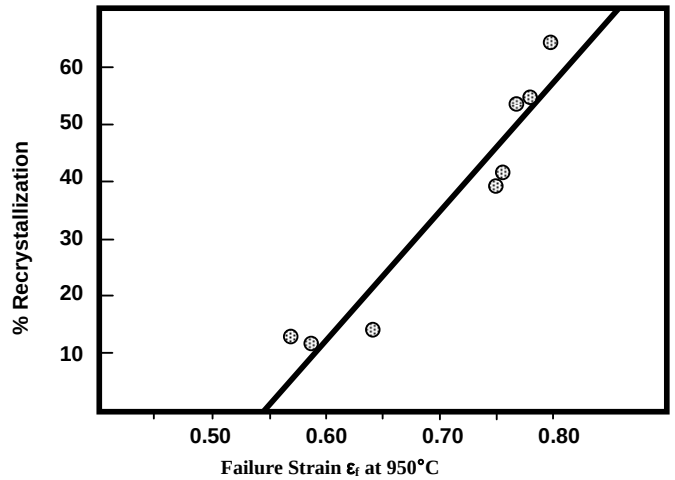

Figure 9. Relationship between recrystallization and failure strain, ε_f at 950°C.

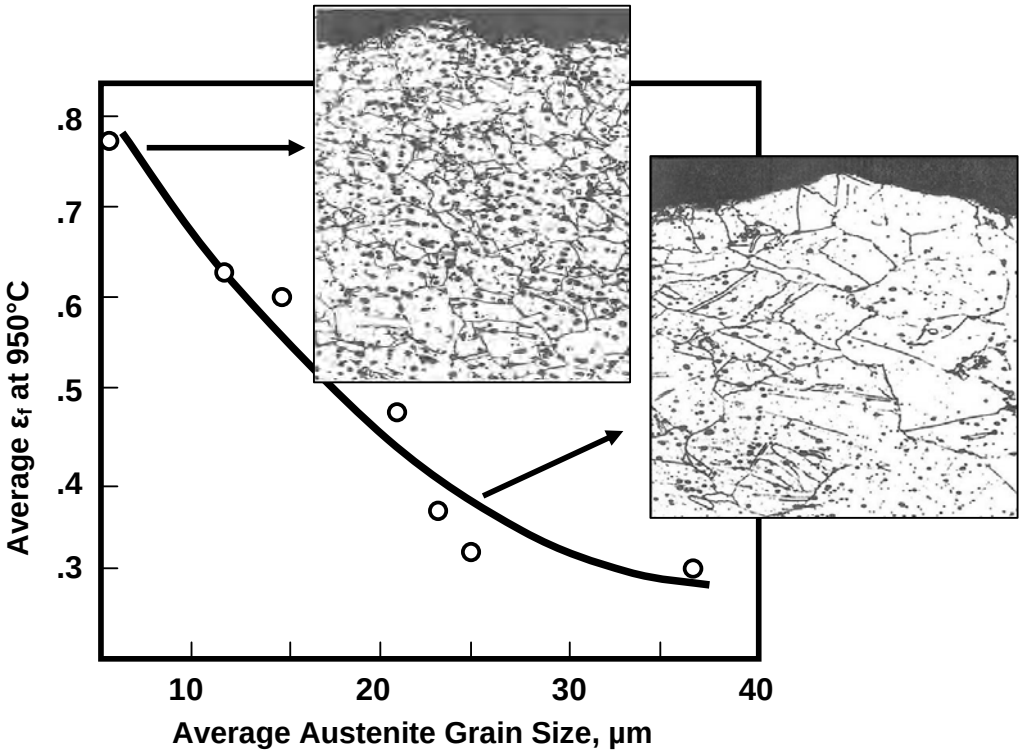

Figure 10. Relationship of austenite grain size and hot ductility.

The next question is how the δ-ferrite might act to lower the extent of recrystallization. Palmiere et al., following Zener [14], has shown that particles can suppress static recrystallization provided their number (volume fraction) is sufficiently high and their average size is sufficiently small. These particles exert a pinning or retarding force on a potentially moving boundary, whose motion would be a step in the recrystallization process. The magnitude of this pinning force can be estimated by Equation 1, [15]

$$F_{PIN}^{SB} = 3\sigma f_V l (2\pi r^2)^{-1} \qquad (1)$$

where σ is the interfacial energy of the moving boundary, f_V is the volume fraction of particles, l is the inter-particle spacing and r is the particle radius of the δ-ferrite. When this pinning force approaches the driving force for recrystallization (stored energy of deformation), it will suppress the amount of recrystallization that will occur. Hence, anything that acts to raise the δ-ferrite content will also act to reduce both the extent of recrystallization and the subsequent hot ductility. The relationship between retained δ-ferrite and recrystallization or hot ductility has been observed in numerous studies [4,16-18]

Sulfur, being a ferrite former when present as solute, will increase the amount of retained δ-ferrite. In addition, the MnS particles that would form at higher sulfur levels would also act to suppress recrystallization. There was no evidence that supported MnS acting as a void former in the ductile fracture process. The main role of S appeared to be to help suppress recrystallization, perhaps by causing an increase or abetting in the pinning effect of the δ-ferrite islands on the boundaries of the columnar γ grains.

Summary and Conclusions

- There appears to be a direct relationship between hot ductility and sliver formation. In this study, the conditions that lead to higher hot ductility at 950°C also resulted in lower sliver formation.
- Higher hot ductility, as measured in the current experiments, was achieved by achieving (a) higher degrees of recrystallization of the dendritic/columnar grain structure and (b) smaller recrystallized grain size, prior to testing.
- The degree of recrystallization in T304 was shown to be strongly controlled by the
- δ-ferrite present prior to testing. The pinning force exterted by the δ-ferrite is responsible for this suppression. Lower retained δ-ferrite contents would lead to easier recrystallization of the dendritic/columnar grain structure.
- Because of solidification and cooling irregularities in the continuous caster, the δ-ferrite content was very high in the gutter regions, near the edges of the broad slab faces. This set the stage for hot ductility problems later in the processing. The effect was magnified at increased sulfur levels.
- Sliver resistance can be improved by strengthening the dendritic/columnar grain boundaries, by reducing the deleterious elements in the steel and/or by adding boundary-enhancing elements such as boron.
- Sliver resistance can also be improved by allowing an extensive amount of recrystallization to occur prior to final hot rolling in the finishing mill.

References

[1] ASM Metals Handbook, 8th Edition, Vol. 8, ASM, Metals Park, OH, 1973, p425.
[2] R. J. Castro and J. J. de Cadenet, Welding Metallurgy of Stainless and Heat Resistant Steels, Cambridge University Press, Cambridge, 1974
[3] A. J. DeArdo, Basic Metals Processing Research Institute, Department of Mechanical Engineering and Materials Science, University of Pittsburgh, Unpublished research, 1997.
[4] B. Ahlblom and R. Sandstorm, Int. Met. Rev., 27 (1982), 1-27.
[5] H. J. McQueen and J. J. Jonas, J. Appl. Metalworking, 3 (1984)
[6] N. D. Ryan, H. J. McQueen and J. J. Jonas, Can. Met. Q., 22 (1983), 369-78.
[7] U. Svenson, The Hot Deformation of Austenite, J. B. Balance, ed., AIME, New York, (1977), 499-516.
[8] D. Hengerer, Radex Rundschau, 1 (1977), 72-82.
[9] W. J. McG Tegart, Ductility, ASM, Metals Park, Ohio, (1968), 133-177.
[10] F. E. White and C. Rossard, Deformation Under Hot Working Conditions, Iron and Steel Institute, London (1968), 14-20.
[11] F. E. White and C. Rossard, Rev. Met., 63 (1966), 991-998.
[12] E. Shapiro and G. E. Dieter, Met. Trans., 1 (1970), 1711-1719, 2 (1971) 1385-1391.
[13] M. D. Coward, G. J. Richardson and C. M. Sellars, Met. Tech., 3 (1976), 550-555.
[14] C. Zener, Trans. AIME, 1949, **175**, 15.
[15] A. J. DeArdo, C. I. Garcia and E. J. Palmiere, "Thermomechanical Processing of Steel," Metals Handbook, American Society for Metals, Metals Park, OH, Vol. 4, (1991), 237.
[16] C. H. Sellars and W.J. McG. Tegart, Int. Met. Rev., 17 (1972), 1-24.
[17] A. Gueussier and R. J. Castro, Rev. Met., 55 (1958), 1023-1048.
[18] J. H. Decroix, A. M. Neveu and R. J. Castro, Deformation Under Hot Working Conditions, Iron and Steel Institute, London (1968), 135-144.